Journal of Catalysis 345 (2017) 53–69

Contents lists available at ScienceDirect

Journal of Catalysis

journal homepage: www.elsevier.com/locate/jcat

# Effect of temperature and branching on the nature and stability of alkene cracking intermediates in H-ZSM-5 ☆

P. Cnudde, K. De Wispelaere, J. Van der Mynsbrugge, M. Waroquier, V. Van Speybroeck *

*Center for Molecular Modeling, Ghent University, Technologiepark 903, B-9052 Zwijnaarde, Belgium*

ARTICLE INFO

*Article history:*
Received 12 August 2016
Revised 7 November 2016
Accepted 8 November 2016

*Keywords:*
Metadynamics
Molecular dynamics
Density functional theory
Zeolite ZSM-5
Catalysis
Alkene adsorption

ABSTRACT

Catalytic cracking of alkenes takes place at elevated temperatures in the order of 773–833 K. In this work, the nature of the reactive intermediates at typical reaction conditions is studied in H-ZSM-5 using a complementary set of modeling tools. Ab initio static and molecular dynamics simulations are performed on different $C_4$— $C_5$ alkene cracking intermediates to identify the reactive species in terms of temperature. At 323 K, the prevalent intermediates are linear alkoxides, alkene π-complexes and tertiary carbenium ions. At a typical cracking temperature of 773 K, however, both secondary and tertiary alkoxides are unlikely to exist in the zeolite channels. Instead, more stable carbenium ion intermediates are found. Branched tertiary carbenium ions are very stable, while linear carbenium ions are predicted to be metastable at high temperature. Our findings confirm that carbenium ions, rather than alkoxides, are reactive intermediates in catalytic alkene cracking at 773 K.


## 1. Introduction

Acid zeolite catalyzed alkene cracking processes are widely applied in chemical industry for the production of gasoline and light olefins, e.g., fluid catalytic cracking (FCC), methanol-to-olefins (MTO), . . . [1–6]. Recently, the expanding shale gas recovery and rising interest in sustainable chemical processes, based on alternative feedstocks, have seriously impacted the light olefin economy. To meet the increasing propene and (to a lesser extent) ethene demand, on-purpose producing technologies have become economically interesting [7–10]. A promising technology is zeolite-catalyzed cracking of the less valuable $C_4$ through $C_8$ alkene fraction. Although cracking is generally accepted to occur through a β-scission mechanism of carbenium ions [5,11–15], the precise nature of the adsorbed intermediates remains unresolved up to date. Especially at operating conditions (773–833 K), limited information is known on the nature of alkene cracking intermediates.

Upon adsorption of the olefin in the zeolite channels, four possible intermediates (Scheme 1) can be formed, namely (1) a physisorbed van der Waals complex characterized by only dispersion interactions between the alkene and the zeolite wall; (2) a physisorbed π-complex in which the C=C double bond interacts with the Brønsted acid site (BAS) of the catalyst; (3) a chemisorbed carbenium ion formed upon protonation of the alkene; and (4) a chemisorbed alkoxide, covalently bound to a framework oxygen. While the existence of a stable physisorbed π-complex has been generally accepted [16–18], the nature of the chemisorbed state upon alkene protonation – a free carbenium ion or an alkoxide – is still debated. Many studies presume that covalently bound alkoxide intermediates are formed as cracking reactants [18–25].

Because of the high reactivity of alkenes, even at low temperature, studying olefin adsorption is challenging and experimentally tracking the often short-lived intermediates is extremely hard [26,27]. To date, the existence of small linear alkyl carbenium ions could not be proven by spectroscopic techniques due to their fleeting nature. In the 1990s, several $^{13}C$ NMR [28–34] and FT-IR spectroscopy studies [35–41] were carried out to identify alkene intermediates in H-ZSM-5 and other acid zeolites. In all of these, alkoxide species were observed as long-living intermediates. No non-aromatic carbenium ions were found freely in the zeolite pores in a temperature range of 150–370 K. Therefore carbenium ions were suggested to behave as short-living transition states rather than reaction intermediates [28,31]. Kondo et al. showed the existence of branched $C_8$ alkoxide dimers below room temperature by IR spectroscopy on adsorption and dimerization of isobutene in H-ZSM-5, although formation of secondary $C_8$-alkoxides prevailed over tertiary ones because of steric constraints [40,41]. Interestingly, no t-butoxide nor t-butyl cation intermediate could be identified. However, at actual cracking temperatures, the

☆ This contribution is part of the virtual issue "30 years of the International Conferences on Theoretical Aspects of Catalysis (ICTAC)".

* Corresponding author.
*E-mail address:* veronique.vanspeybroeck@ugent.be (V. Van Speybroeck).

http://dx.doi.org/10.1016/j.jcat.2016.11.010
0021-9517/

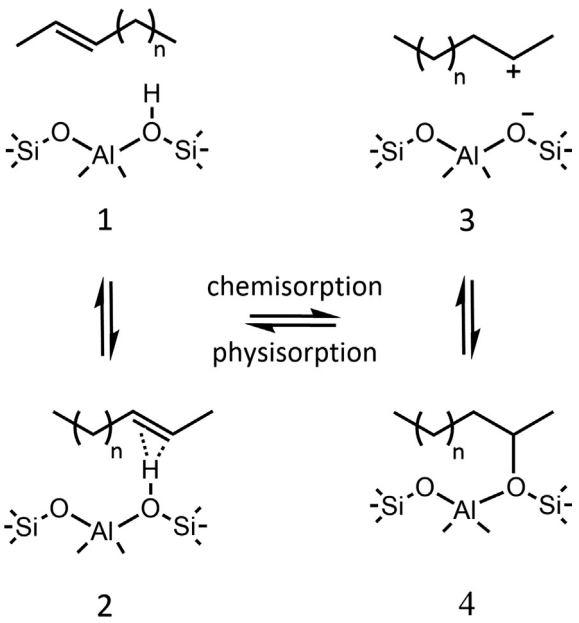


**Scheme 1.** Four adsorption states of a 2-alkene – 1: Van der Waals complex, 2: π-complex, 3: carbenium ion, 4: alkoxide.

situation may be different than at the relatively low temperatures employed in these spectroscopy studies.

Apart from these experimental studies, alkene adsorption has been mainly addressed theoretically. Early quantum chemical studies, carried out on small cluster models consisting of only a few T atoms, supported the hypothesis that chemisorbed alkoxides are highly stable, while secondary or tertiary carbenium ions are non-existent in the zeolite pores except as transition states [21,42–48]. However, these small cluster models lack a proper description of long-range interactions and the zeolite confinement. Studies on larger clusters or periodic models that account for the zeolite cavity concluded that $C_3$—$C_6$ alkoxides indeed exist as the most stable adsorption state, although their relative stability compared to physisorbed states at 0 K may not be as high as initially expected [18,20,49–53]. This observation resulted in the assumption that alkoxides can act as reactive intermediates, which rearrange over transition states of ionic nature [20,49].

The zeolite topology and local geometry of the active site can complicate alkoxide and facilitate carbenium ion pair formation since the stability of alkoxides is influenced by steric constraints introduced by the pore dimensions [54–58]. Some computational studies rationalized the possibility of persistent carbenium ions in the zeolite pores [55,59–63]. Nicholas and Haw established an empirical relationship stating a stable carbenium ion can exist in an H-zeolite if the neutral compound has a gas-phase proton affinity (PA) of 874 kJ/mol or higher [64,65]. The authors also suggested that at high temperature, species with a PA around the critical value are likely to form transient, short-living cations. Later studies confirmed for different zeolites that the proton affinity of the neutral alkene correlates with the energy difference between the carbenium ion and the alkene [57,66]. Furthermore, Benco et al. showed that the relative stability of protonated olefins also depends on the carbon number [60]. Carbenium ions may be stabilized from a certain length of the olefin, resulting from a proper accommodation of the positive charge in the zeolite environment [60,67,68]. In a recent study, we identified pentyl carbenium ions as metastable intermediates on the free energy surface at 323 K using a combination of static and dynamic methods [69].

Isobutene adsorption is an ideal benchmark system that received special attention in a series of theoretical studies [54,58,61,70–72]. Alkoxide stability was found to diminish from very stable primary to less stable tertiary alkoxides, which is opposite to the stability order of carbenium ions. It has been argued that due to steric constraints between the methyl groups and the zeolite wall, the *tert*-butyl carbenium ion can become relatively more stable than *tert*-butoxide [19,54,55,72–74]. Tuma and Sauer were the first to perform periodic DFT calculations on H-FER including entropy effects at finite temperature [70]. They concluded that although the *tert*-butyl carbenium ion is electronically least favored, the entropic penalty for *tert*-butoxide formation renders the tertiary cation more stable than the alkoxide for temperatures higher than 120 K. Later, the authors extended their study using a hybrid MP2:DFT method to re-evaluate the stability of the $C_4$ species when dispersion interactions are included [61,74]. The observed behavior of *tert*-butyl species on H-ZSM-5 in function of temperature has been confirmed by Nguyen et al. while accounting for dispersion interactions and entropy effects [58]. Recently, Dai et al. found additional evidence for the existence of the *tert*-butyl cation by combining NMR spectroscopy with DFT calculations [71].

To the best of our knowledge, the nature of linear and branched alkene intermediates at process temperatures has not yet been unraveled. Nevertheless, such insight is mandatory for further optimizing the process and catalyst. In this work, we aim to clarify the precise nature of adsorbed linear and branched $C_4$—$C_5$ intermediates at actual alkene cracking conditions. As a catalyst, we chose H-ZSM-5, which was proven to be one of the most effective industrial catalysts in light olefin production due to its optimal balance between conversion, selectivity and coke formation stability [13,75,76]. Schemes 2a and 2b depict the possible intermediates upon adsorption of $C_4$ and $C_5$ alkenes respectively. Primary carbenium ions are not considered as candidate intermediates in this work due to their highly unstable nature [12,22,77,78]. We investigate the differences in stability between linear and branched adsorbate states and the influence of temperature by comparing three different cases – 323 K, a typical temperature for spectroscopy experiments, 573 K, an intermediate temperature and 773 K, a typical cracking temperature. To this end, we applied a combination of static DFT calculations and molecular dynamics simulations which inherently account for entropy and finite temperature effects as well as the mobility of the adsorbates. Metadynamics simulations were performed to sample transitions between the different intermediate states, separated by non-negligible free energy barriers. Using the advantages of these three techniques allows assessing the stability differences at operating conditions both qualitatively and quantitatively. MD simulations have been successfully combined with static calculations and free energy methods to study adsorption properties and reactions of hydrocarbons in zeolite materials [27,68,79–86]. For the problem at hand, a complementary approach between static and dynamic techniques is applied to acquire detailed knowledge on the nature of the intermediates.

## 2. Methodology

### 2.1. Zeolite model

All static and dynamic density functional theory (DFT) calculations are performed on a periodic model of the H-ZSM-5 catalyst, fully accounting for the confinement in the zeolite pores. H-ZSM-5 exhibits the MFI topology which consists of intersecting straight (5.3 Å × 5.6 Å) and sinusoidal (5.1 Å × 5.5 Å) channels. The orthorhombic unit cell contains 289 atoms (96T atoms) and a single Brønsted acid site. The substitutional Al defect is situated at the T12 position, i.e. at the intersection of the straight and sinusoidal

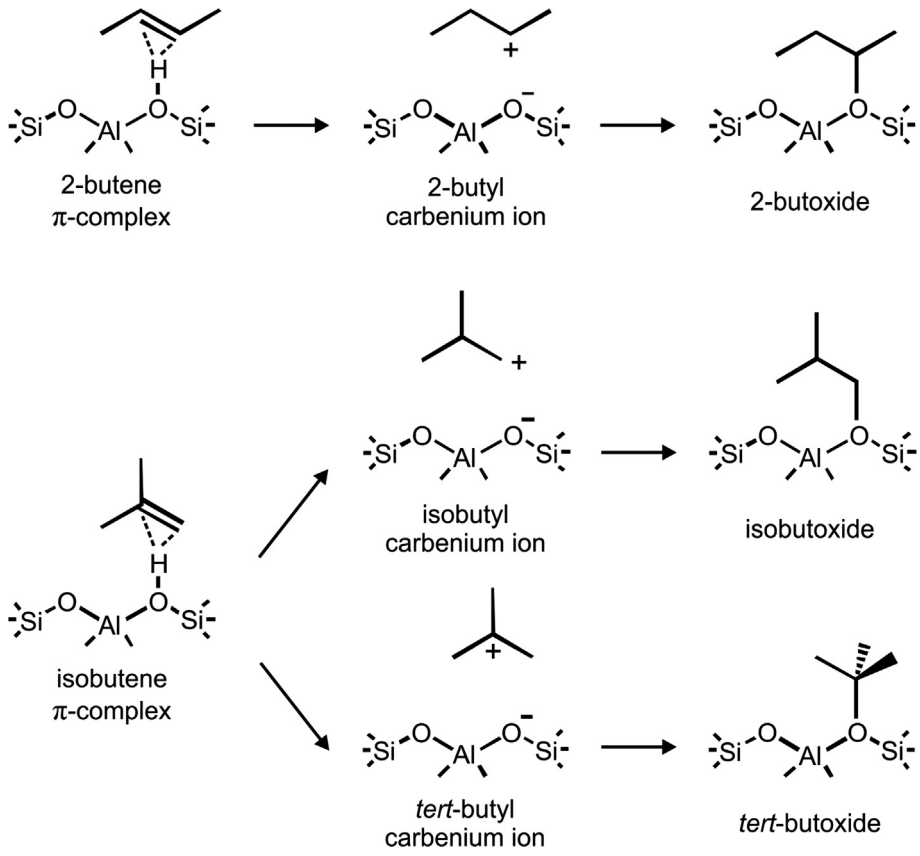


**Scheme 2a.** Adsorption states of linear and branched butenes.

channel, providing optimal space for the adsorbates and subsequent reactions. The charge compensating proton is located at the $O_{20}$ position (see Fig. 1). The alkoxide species are also bound to framework oxygen $O_{20}$.

### 2.2. Static calculations

Static periodic DFT calculations have been performed with the Vienna Ab Initio Simulation Package (VASP) [87–90]. First, geometry optimizations using the PBE functional with additional Grimme D3 dispersion corrections [91] have been carried out. A conjugate gradient method allows the ions to relax into the ground state. The self-consistent field (SCF) convergence criterion was set at $10^{-5}$ eV and a plane wave kinetic energy cutoff of 600 eV was applied together with the projected augmented approximation (PAW) [92,93]. The framework was allowed to fully relax during the geometry optimization. Additionally, an energy refinement using Tkatchenko's many body dispersion (MBD) scheme with iterative Hirshfeld partitioning [94,95] was performed. To verify that the optimized geometries correspond to local minima, a normal mode analysis was performed. To obtain the frequencies, a partial Hessian vibrational analysis (PHVA) [96–98] was carried out on an 8T cluster around the acid site of the framework and the adsorbate. Thermal corrections were calculated within the harmonic oscillator (HO) approximation using the in-house developed TAMkin software [99]. Adsorption enthalpies, entropies and Gibbs free energies at the desired temperature are determined as follows:

$$\Delta X_{ads} = X(\text{adsorption complex}) - X(\text{empty zeolite}) - X(\text{isolated guest molecule})$$

in which $X$ stands for electronic energy at 0 K (E), enthalpy (H), entropy (S) or Gibbs free energy (G). In each individual adsorption complex the zeolite lattice adapts to the size and position of the guest molecule in the channel intersection. To ensure the same truncated basis set is used, the empty zeolite – obtained by cutting out the adsorbate – is re-optimized by keeping the cell volume and cell shape constant. In this approach, the influence of local lattice deformations is also eliminated.

### 2.3. Ab initio molecular dynamics simulations

Molecular dynamics (MD) simulations were carried out with the CP2K software package [100,101] using the revPBE [102] functional with additional Grimme D3 dispersion corrections [91]. The DZVP-GTH basis set [103] was used, which is a combination of Gaussian basis functions and plane waves (GPW) [104,105] with a cutoff energy of 320 Ry. The time step for integrating the equations of motion was set to 0.5 fs. The system was simulated in the NVT ensemble at a temperature of 323, 573 or 773 K, which is controlled by a chain of five Nosé-Hoover thermostats [106,107]. Cell parameters are determined from a preliminary 5 ps run on the empty zeolite in the NPT ensemble at the corresponding temperature and a pressure of 1 bar, which is controlled by an MTK barostat [108] (see Table S.1 of the Supplementary Material). Next, the actual NVT simulation was performed starting with a 5 ps equilibration run to initialize the system, followed by the production run of 100 ps to obtain a sufficient sampling of the phase space. The unit cell of ZSM-5 is quite large and flexible; hence, we opted to perform NVT simulations in which the framework is still allowed to relax and adapt to the size and position of the adsorbate, but the unit cell volume is kept constant. In

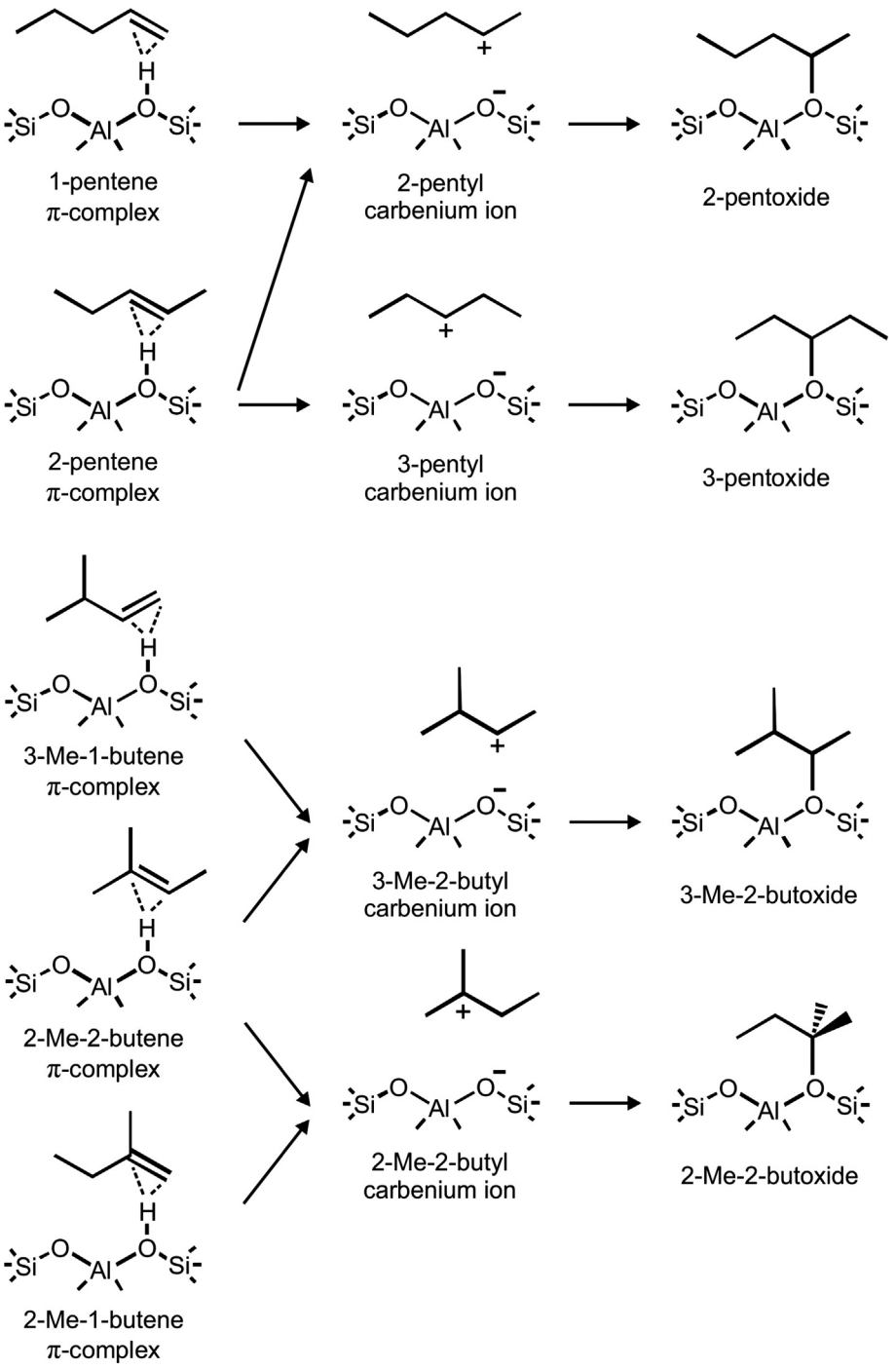


**Scheme 2b.** Adsorption states of linear and branched pentenes.

addition, NpT simulations are computationally much more expensive compared to NVT simulations.

If rapid rearrangements of the adsorbate occurred in the equilibration run or the first few picoseconds of the production run, the simulation was repeated three times with random initial velocities to ensure that not merely a rare event was sampled. We established a criterion based on some characteristic geometrical distances to distinguish between the different intermediate states. For a carbenium ion, all H—$O_z$ distances should be larger than 1.25 Å; otherwise, a physisorbed alkene is sampled. The latter is classified as a π-complex if the distances between the acid proton and the double bond carbon atoms are both smaller than 2.85 Å, if not the adsorbate is a van der Waals complex. The adsorbate is considered an alkoxide if the covalent C—$O_z$ bond with the framework does not exceed 1.9 Å.

### 2.4. Metadynamics simulations

In our previous work [69], we have shown that free energy barriers for the transition between the different intermediates are too high to spontaneously overcome in regular MD. Metadynamics (MTD) is a powerful technique to accelerate the sampling of rare

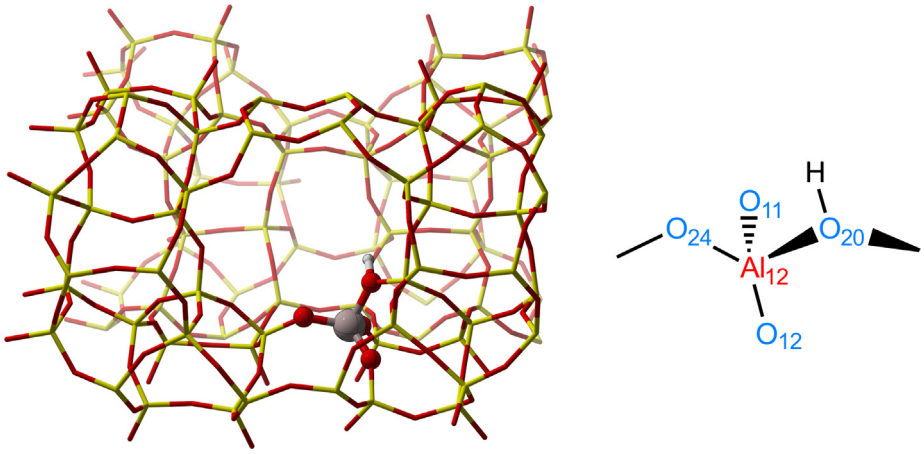


**Fig. 1.** H-ZSM-5 unit cell with indication of the Al substitutional defect and the acid site.

events and determine the minimum energy path of activated processes on the multi-dimensional free energy surface [109,110]. The MTD method allows sampling specific regions on the free energy surface by properly selecting a (set of) collective variable(s) (CV) [109–111]. In this work, simulations were performed in the NVT ensemble at typical cracking conditions (773 K) with the same settings as in the MD simulations. The MTD simulation is biased by regularly spawning Gaussian hills along the chosen collective variable(s), which are defined by coordination numbers (CN):

$$CN = \sum_{i,j} \frac{1-(r_{ij}/r_0)^{nn}}{1-(r_{ij}/r_0)^{nd}}$$

in which the sum runs over two sets of atoms $i$ and $j$ with $r_{ij}$ the interatomic distance between atoms $i$ and $j$ and $r_0$ a reference distance. In this study, the parameters $nn$ and $nd$ are set at 6 and 12 respectively. All simulations performed in this work use a single CV (1D MTD), shown in Fig. 2. For the alkene protonation, the collective variable CV1 is defined by a difference of CNs: CN(C—H) – CN(H—O) to describe proton transfer from the zeolite to the hydrocarbon. A reference distance of 1.25 Å was selected, which lies around typical transition state values of bond distances for (de)protonation reactions. For the formation of alkoxide species, the CN (C—O) is used as CV2 with a reference distance of 2.1 Å.

Quadratic walls were applied to force the system to remain in the particular area of interest on the free energy surface. More technical information can be found in Section S6 of the Supplementary Material. Isomerizations between different cationic states were prevented and the same carbon atom was ensured to be protonated each time. Hills with a width of 0.035 were spawned every 100 time steps. The initial hill height of 2 kJ/mol was reduced by 50% upon each recrossing of the barrier to improve convergence of the FES. The simulations were continued until the height of the additional hills no longer influences the resulting free energy profile. Based on the sum of the spawned Gaussian hills, the 1D free energy profile of the reaction was reconstructed. Once the free energy profiles were determined, free energy activation barriers $\Delta G^{\ddagger}$ were computed as the difference between the free energy of the transition state (TS) and the minimal free energy in the reactant or product valley.

$$\Delta G^{\ddagger}_{fwd} = G_{max,TS} - G_{min,reactant}$$

$$\Delta G^{\ddagger}_{bwd} = G_{max,TS} - G_{min,product}$$

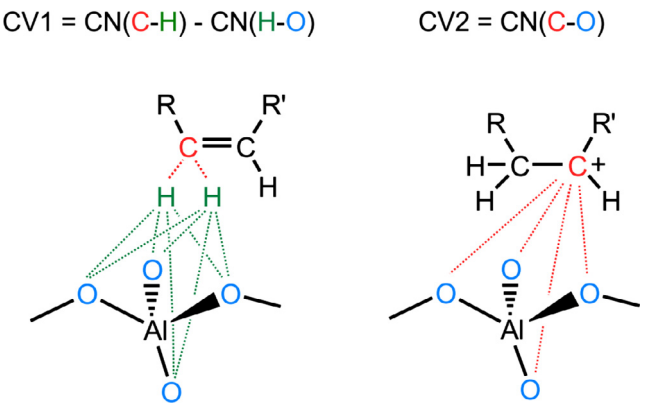


**Fig. 2.** Schematic visualization of the collective variables used in the 1D metadynamics simulations for alkene protonation (CV1) and for alkoxide formation (CV2).

## 3. Results and discussion

### 3.1. Adsorption behavior of C4 and C5 species within a static approach

To analyze the relative stability of all $C_4$ and $C_5$ intermediates, first, static periodic calculations at the PBE-D3 level of theory have been carried out on the species shown in Schemes 2a and 2b. Initial geometries for the various adsorption states were taken from short MD runs of about 10 ps, starting from unbiased adsorbate positions. This proved to be an efficient procedure to localize distinct minima on the complex potential energy surface of these systems as shown in previous work [69]. For several $C_4$ species, multiple local minima have been identified and only the most stable geometries were retained (cf. Section S3 in the Supplementary Material). In Table 1, electronic energies, enthalpies and free energies of adsorption at 323 K and 773 K are reported with the empty framework and 2-butene (for the $C_4$ species) or 1-pentene (for the $C_5$ species) in gas phase as reference state. Next to the PBE-D3 calculations, also single point revPBE-D3 calculations have been performed (see Table S.4. in Supplementary Material) to allow for a proper comparison with the MD simulations. The energy differences between both levels of theory are negligibly small (less than 4 kJ/mol).

Regardless of which species is adsorbed, the physisorbed π-complex is observed to be more stable than the chemisorbed alkoxide or carbenium ion, irrespective of temperature. This effect is most pronounced for the linear alkenes as previously reported by Hajek et al. [69]. The electronic adsorption energies – obtained with the PBE-D3 method – of the linear 2-butene π-complex and

**Table 1**
Electronic energies, adsorption enthalpies and free energy differences for the various adsorption states of C4 and C5 species in H-ZSM-5 at temperature 323 K and 773 K. All energies are relative with respect to the empty framework and 2-butene (g) for the C4-species or 1-pentene (g) for the C5-species. LOT electronic energies: PBE-D3.

| | | 0 K | 323 K | | 773 K | |
|---|---|---|---|---|---|---|
| | Species | $\Delta E$ kJ/mol | $\Delta H$ kJ/mol | $\Delta G$ kJ/mol | $\Delta H$ kJ/mol | $\Delta G$ kJ/mol |
| **$C_4$** | | | | | | |
| LINEAR | 2-butene (g) | 0 | 0 | 0 | 0 | 0 |
| | 2-butene π-complex | −107 | −102 | −51 | −96 | 18 |
| | 2-butyl carbenium ion | −18 | −18 | 34 | −11 | 103 |
| | 2-butoxide | −101 | −90 | −24 | −86 | 66 |
| BRANCHED | isobutene (g) | −3 | −3 | −2 | −3 | −1 |
| | isobutene π-complex | −106 | −103 | −52 | −97 | 15 |
| | *tert*-butyl carbenium ion | −83 | −86 | −34 | −79 | 36 |
| | *tert*-butoxide | −90 | −80 | −13 | −75 | 81 |
| | isobutoxide | −96 | −83 | −18 | −80 | 72 |
| **$C_5$** | | | | | | |
| LINEAR | 1-pentene (g) | 0 | 0 | 0 | 0 | 0 |
| | 2-pentene (g) | −13 | −15 | −15 | −14 | −16 |
| | 1-pentene π-complex | −119 | −114 | −56 | −108 | 23 |
| | 2-pentene π-complex | −134 | −130 | −72 | −124 | 5 |
| | 2-pentyl carbenium ion | −48 | −49 | 6 | −42 | 80 |
| | 3-pentyl carbenium ion | −43 | −38 | 13 | −31 | 80 |
| | 2-pentoxide | −124 | −113 | −46 | −109 | 46 |
| | 3-pentoxide | −119 | −107 | −40 | −104 | 53 |
| BRANCHED | 2-Me-2-butene (g) | −13 | −14 | −15 | −14 | −15 |
| | 2-Me-1-butene (g) | −22 | −25 | −27 | −24 | −32 |
| | 2-Me-1-butene π-complex | −128 | −125 | −69 | −118 | 6 |
| | 3-Me-1-butene π-complex | −114 | −110 | −56 | −104 | 17 |
| | 2-Me-2-butene π-complex | −145 | −143 | −87 | −137 | −13 |
| | 3-Me-2-butyl carbenium ion | −55 | −57 | 0 | −49 | 75 |
| | 2-Me-2-butyl carbenium ion | −113 | −113 | −60 | −106 | 10 |
| | 3-Me-2-butoxide | −124 | −114 | −45 | −110 | 50 |
| | 2-Me-2-butoxide | −111 | −102 | −36 | −97 | 54 |

2-butoxide are comparable (6 kJ/mol energy difference). Both states are substantially more stable than the 2-butyl carbenium ion. At higher temperatures, the entropic penalty of the covalent C—O bond renders the π-complex relatively more stable than 2-butoxide. At 773 K, the free energy of adsorption of the physisorbed 2-butene π-complex is 48 kJ/mol lower than the 2-butoxide which is in turn 37 kJ/mol more stable than the 2-butyl carbenium ion. The free energy difference of 85 kJ/mol between the 2-butyl carbenium ion and the 2-butene π-complex indicates that the linear butyl carbenium ion will most likely not exist, even at elevated temperatures.

A different conclusion arises for the branched $C_4$ intermediates. Tertiary carbenium ions are much more stabilized than their linear analogues, albeit π-complexes still remain the most stable species at all temperatures. At 0 K, the *tert*-butyl cation is 65 kJ/mol more stable than the 2-butyl cation and almost equally stable (7 kJ/mol energy difference) than *tert*-butoxide. The isobutene π-complex has the lowest adsorption energy of the branched $C_4$ intermediates, followed by the primary isobutoxide. The entropic contribution to the free energy of alkoxide adsorption (see Table S.2 in the Supplementary Material), however, is larger compared to carbenium ions and π-complexes, thus reflecting a change of the stability order at 773 K. The *tert*-butoxide has a high free energy of adsorption at elevated temperature (81 kJ/mol) and is much less stabilized than the *tert*-butyl cation (36 kJ/mol). Note that all adsorption free energies are quite high at 773 K, indicating that entropy effects may disfavor the formation of a tightly bound physisorbed or chemisorbed intermediate. This will be further investigated by molecular dynamics simulations (*vide infra*).

In Table 2, the results of our calculations are compared to previous computational studies on isobutene adsorption in different zeolites. Dispersion interactions with the zeolite framework form the main contribution to the adsorption energies of the $C_4$ intermediates. Our results vary significantly from the results obtained by Tuma and Sauer, who performed PBE calculations without van der Waals corrections [70]. At that time, periodic DFT calculations with advanced functionals and inclusion of dispersion interactions were not feasible; hence, their results should be regarded within this perspective. In later work, the same authors performed very accurate calculations with a hybrid MP2:DFT method on the stability of $C_4$ species in H-FER, which are largely different from their dispersion-free calculations [61,74]. Using the hybrid method, they located stable states for all isobutene intermediates, including the *tert*-butyl cation although the relative stabilities differ from the results reported herein. Especially, the *tert*-butyl cation is substantially more stable in the PBE-D3 calculations. The origin of this discrepancy which is the most pronounced for the cation (−80 kJ/mol with PBE-D3 vs. −17 kJ/mol with MP2:PBE) is probably multifold. It can be partly due to an overestimation of the stability of the ion-pair by PBE, as stated by Kerber et al. [112]. We therefore also performed single-point calculations with the hybrid functional B3LYP+D3 (see Table 2) to partly resolve this discrepancy. The *tert*-butyl cation is indeed about 10 kJ/mol less stable compared to the PBE-D3 results. The qualitative features, however, remain more or less the same.

In H-ZSM-5, also a series of adsorption energies were reported, which vary substantially, depending on the applied methodology. Based on 72T cluster calculations at the ONIOM(M06-2X/6-31G(d):AM1) level of theory, Fang et al. [57] predicted an adsorption energy for the *tert*-butyl carbenium ion of −13 kJ/mol. Our results are in line with the periodic PW91-D//PW91 calculations by Nguyen et al. [58] which is expected since they performed periodic calculations with a similar level of theory. The slight differences (less than 10 kJ/mol) may be attributed to fixed unit cell parameters, a different position of the acid proton ($O_{24}$) or the selection of geometries. We selected a probable configuration from MD sim-

**Table 2**
Comparison of electronic adsorption energies $\Delta E_{ads}$ (kJ mol$^{-1}$) for the intermediates upon isobutene adsorption from the literature.

| | Tuma and Sauer [70] | Tuma et al. [61] | Nguyen et al. [58] | Fang et al. [57] | Dai et al. [71] | Current work | |
|---|---|---|---|---|---|---|---|
| *Framework* | H-FER | H-FER | H-ZSM-5 | H-ZSM-5 | H-ZSM-5 | H-ZSM-5 | |
| *Model* | Periodic | Periodic | Periodic | 72T cluster | Periodic | Periodic | |
| *Methodology* | PBE | MP2:PBE | PW91-D2 | ONIOM (MP2:M06-2X) | BEEF-vdW | PBE-D3 | B3LYP-D3 |
| isobutene π-complex | −7 | −77 | −91 | −75 | −84 | −104 | −107 |
| *tert*-butyl cation | 32 | −17 | −72 | −13 | −44 | −80 | −70 |
| isobutoxide | 24 | −68 | −103 | – | −87 | −93 | −103 |
| *tert*-butoxide | 35 | −41 | −95 | −28 | −59 | −87 | −90 |

ulations, while Nguyen et al. [58] took geometries associated to a specific reaction path for *tert*-butoxide or isobutoxide formation from isobutene. Furthermore, the authors applied the older D2 dispersion corrections [113]. Dai et al. [71] also performed a similar isobutene adsorption study in H-ZSM-5, though applying the BEEF-vdW functional. Their adsorption energies follow a comparable trend as the energies reported in this work, but with a systematic deviation, which may possibly be attributed to the BEEF-vdW functional [71].

For the branched $C_5$ species, analogous observations can be made. The tertiary 2-Me-2-butyl carbenium ion is also characterized by its large negative adsorption energy and becomes more stable than the corresponding alkoxide at low temperature (323 K). Our results again indicate that π-complexes are stable at all temperatures but tertiary carbenium ions might also occur. The particular influence of temperature beyond the HO approximation will be assessed using MD simulations.

To assess the influence of the applied dispersion methodology on the adsorption behavior, the adsorption energies were also obtained with the many body dispersion (MBD) scheme proposed by Tkatchenko (listed in Table S.3 in SI). The results show similar trends compared to the D3 calculations although with systematically lower adsorption strengths (6–10 kJ/mol for π-complexes and carbenium ions). The difference is the least pronounced in the case of the alkoxide species (2–5 kJ/mol), for which the protonated alkene is covalently bonded to the framework and therefore less affected by the choice of dispersion model. In the MBD scheme, dispersion has a lower contribution to the total interaction energy.

Static calculations, however, may be prone to some limitations at elevated temperatures. First, the geometry optimization algorithm only explores the PES in the immediate vicinity of the initial structure. Only a single geometry, corresponding to a specific adsorbate position, is considered, while the PES for alkene adsorption is quite flat and complex, exhibiting many local minima with nearly equal energies [69]. We illustrate this with a few examples for the $C_4$ species. The geometries of the different configurations are shown in Section S3 of the SI. For the linear 2-butene π-complex, a configuration adsorbed in the sinusoidal channel is 5 kJ/mol lower in electronic energy than a configuration adsorbed in the straight channel. A second example is the isobutene π-complex for which the different local minima yield electronic energy differences up to 13 kJ/mol. Also, the *tert*-butyl carbenium ion species show an electronic energy spread of 16 kJ/mol. Furthermore, due to different entropy estimates for the selected configurations, the Gibbs free energy spread increases with temperature and already amounts to ca. 20 kJ/mol at 773 K. Bučko et al. reported a similar observation for propane cracking in chabazite [84].

Secondly, the 0 K potential energy surface may differ significantly from the free energy surface at finite temperature. For linear pentenes, we previously showed that the physisorption enthalpy of the π-complex is overestimated in the static approach since the optimized geometry is located too closely to the BAS [69]. Göltl and coworkers also found a considerable variation in adsorption energies of short alkanes in chabazite, even at room temperature [68]. Furthermore, applying the harmonic oscillator (HO) approximation to estimate the free energy at 773 K might result in an underestimation of the mobility, and therefore entropy, of the species. At high temperature, the species usually possess sufficient mobility allowing rapid rearrangements to other configurations [67]. Static calculations may therefore not be fully representative for studying the nature of the reactive intermediates in alkene cracking [79,82].

### 3.2. Evaluating stability differences through MD simulations

To account for conformational freedom and to capture entropy and finite temperature effects in a more realistic way, 100 ps MD simulations are carried out for the different physisorbed and chemisorbed species. The dynamics of butene and pentene intermediates is studied at three temperatures: 323 K, 573 K and 773 K. Special attention will be given to the behavior of carbenium ions. Based on some characteristic geometrical distances, the prevailing intermediates are identified and an estimate of their lifetime is deduced. This yields a qualitative indication of the relative stability of the different intermediates. First, the different linear $C_4$/$C_5$ species are investigated. Secondly, the influence of branching on the stability of intermediates is discussed.

#### 3.2.1. Linear $C_4$ and $C_5$ species

**π-complex simulations**

For all three temperatures, the MD simulations reveal stable π-complex structures. At 323 K, both C=C carbon atoms remain within 2.85 Å of the BAS during 99% of the simulation time; hence, the 2-butene and 2-pentene π-complex states are sampled throughout the entire simulation. Fig. 3 displays the probability distribution of the minimum distance between a double bond carbon atom and the acid proton for 2-butene and 2-pentene. The narrow distributions, centered around 2 Å with a standard deviation of 0.2 Å, clearly confirm that both linear alkenes exist as a π-complex configuration during the entire simulation, indicating the high stability of these physisorbed species at this temperature. This observation is in line with our static calculations.

At the intermediate temperature of 573 K, the distance distributions become asymmetric with a broader tail. The enthalpic stabilization of the π-complex is compensated by an entropic penalty due to constraining the double bond near the acid proton, which causes the π-H interaction with the BAS to break more easily. In the neighborhood of the BAS, regular transitions between the π-complex and the more freely adsorbed alkene, i.e. a physisorbed Van der Waals complex, are observed (ca. 700 transitions during the 100 ps simulation). Due to the increased thermal energy in the system, the small activation barrier between the two physisorbed states can be readily overcome. For 2-butene, the π-complex state is sampled during 51% of the simulation time, while in the remaining 49% a van der Waals complex is sampled. Therefore, two states will probably have a similar free energy at 573 K.

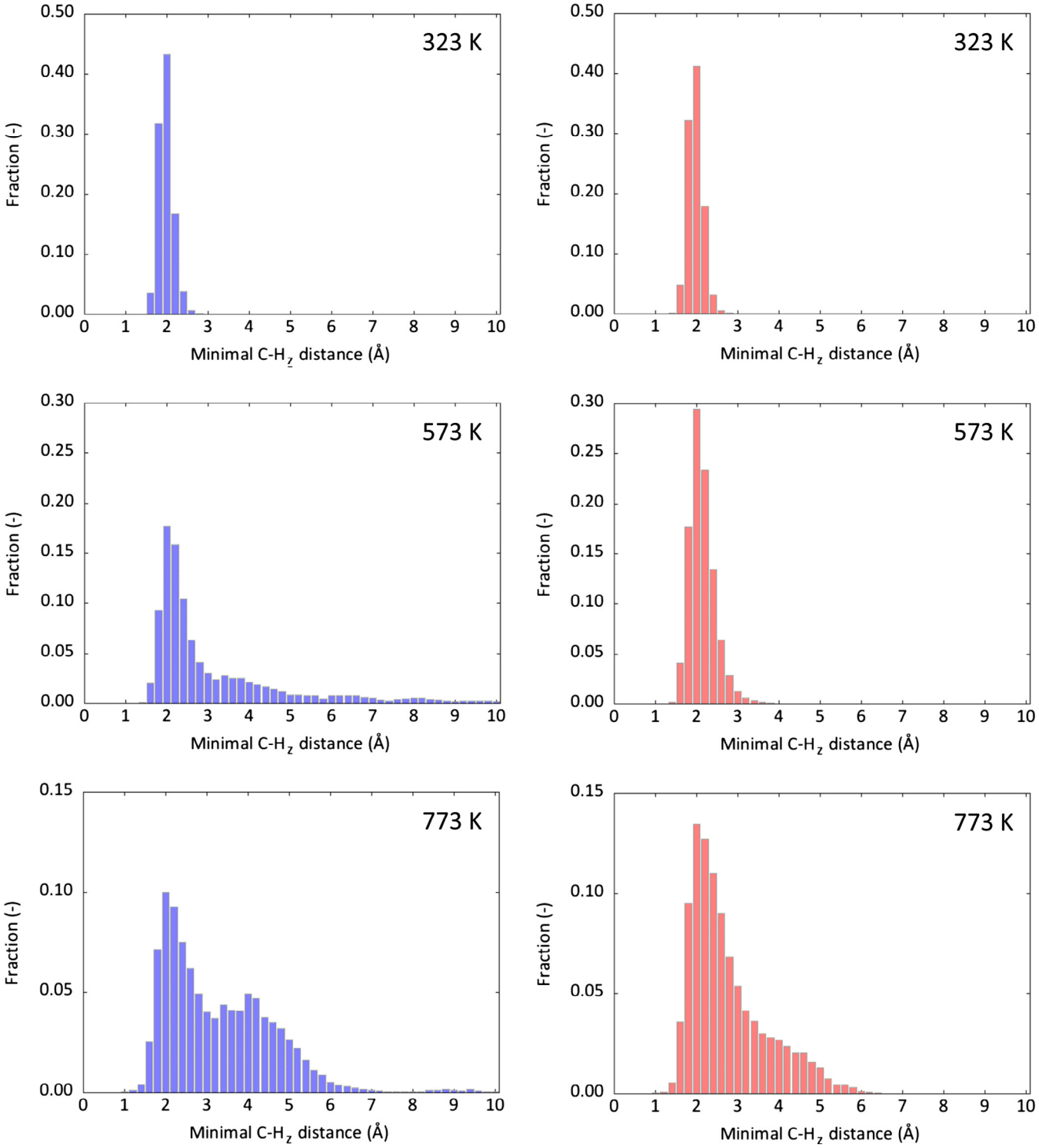


**Fig. 3.** Probability distributions of some critical distances in MD simulations of 2-butene (blue histograms) and 2-pentene (red histograms) π-complexes at 323 K (top), 573 K (middle) and 773 K (bottom) in H-ZSM-5 obtained over 100 ps simulations.

The large C—$H_z$ distances (up to 11 Å) observed during the simulation, which are shown in Figs. 3 and 4, also reveal that the 2-butene species now and then resides at large distance from the BAS, which corresponds to a free alkene diffusing through the zeolite channels. In contrast, the larger 2-pentene seems less prone to diffusion. Indeed, it is sampled 85% as a π-complex and only 15% as a looser van der Waals complex. Again, transitions between the two states take place regularly (ca. 900 transitions).

At a typical cracking temperature of 773 K, analogous trends are observed, though more pronounced. The minimal C—$H_z$ distance is now characterized by a broad distribution for both the 2-butene and 2-pentene π-complex (see Fig. 3). The increased mobility of 2-pentene at this temperature can clearly be noticed, although it drifts less far from the BAS than 2-butene. At this temperature, the adsorbed alkenes can move and rotate freely inside the zeolite channels. The freely adsorbed state is sampled more often than the

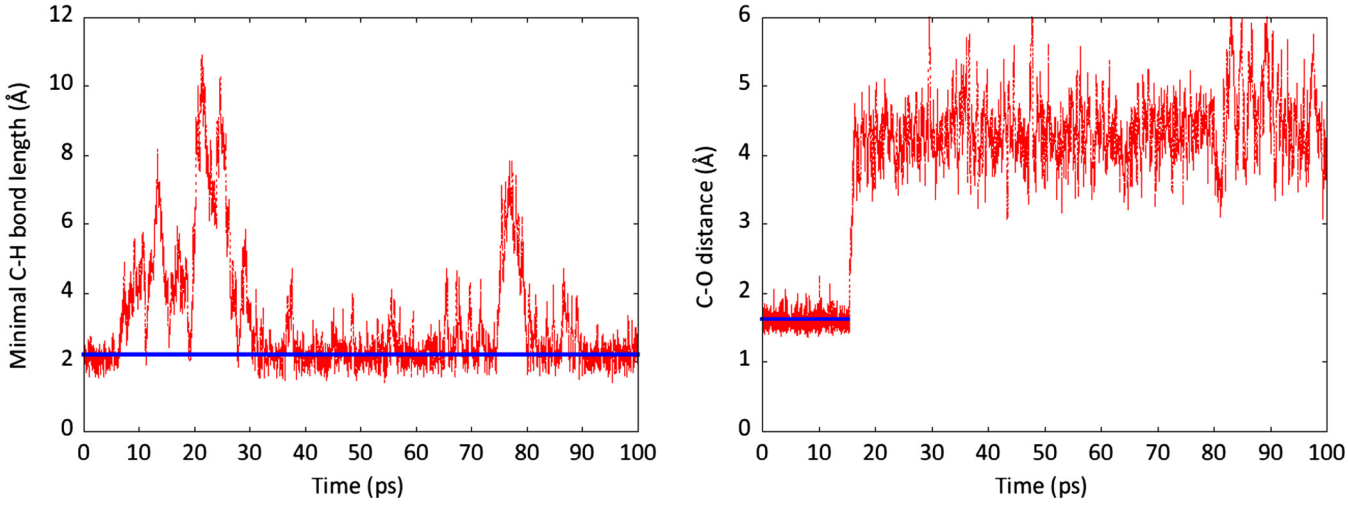


**Fig. 4.** Evolution of the minimal C—$H_z$ distance in the 2-butene π-complex simulation (left) and the C—$O_z$ distance in the 2-pentoxide simulation (right) at 573 K with indication of the average in blue. (3.2 Å for 2-butene π-complex and 1.6 Å for 2-pentoxide.)

π-complex state, at a ratio of 68:32 for 2-butene and 55:45 for 2-pentene. Based on these ratios, the 2-butene van der Waals complex will be slightly lower in free energy compared to the corresponding π-complex. For 2-pentene, on the other hand, the ratio is close to 1, implying that the free energy difference between both physisorbed states will be very small. The transition frequency between the two physisorbed states is comparable to 573 K. Interestingly, a rare protonation of the 2-pentene π-complex to the 2-pentyl carbenium occurred during the MD simulation. The lifetime of this carbenium ion was shorter than 2 ps before a deprotonation to the acid site restored the neutral 2-pentene. In any case, deducing quantitative adsorption energies from MD simulations requires extremely long simulation times since many transitions from one state to another take place in the course of the simulation, thus reducing the effective sampling time of each particular state. An overview of the occurrence of the sampled states during the MD simulations is shown in Fig. 5 for the linear species and Fig. 6 for the branched species. The plots clearly show that linear π-complexes remain stable at lower temperature. However, when starting from a π-complex configuration at higher temperature, transformations into a physisorbed van der Waals complex occur regularly. A complete overview of all MD simulations can be found in Tables S.4 and S.5 in SI.

**Carbenium ion simulations**

From the static calculations (Table 1), the 2-butyl and 2-pentyl carbenium ions were identified as local minima on the potential energy surface. They were however substantially less stable than the corresponding π-complexes and alkoxides. At 323 K (and 573 K), deprotonations systematically occur within the equilibration time (5 ps) of the simulation, demonstrating that linear butyl or pentyl cationic species are unstable intermediates that tend to rearrange quickly into a π-complex (or free alkene). The simulation was repeated three times with different random initial velocities to ensure this observation is not merely coincidental but can be reliably reproduced. Transitions to the 2-butoxide or 2-pentoxide state on the other hand were never observed. In an earlier study [69] we also performed MD simulations on linear pentene intermediates at 323 K, but no carbenium ions were visited in any simulation. The results reported in Ref. [69] support our findings that the interconversion between the π-complex and pentoxide species at 323 K is an activated process which takes place through an extremely short-living cationic intermediate.

At 773 K, a 2-butyl carbenium ion has not been observed. Deprotonation takes place at the start of the equilibration run and the resulting 2-butene remains stable throughout the entire simulation. Instead, deprotonation of the 2-pentyl carbenium ion also takes place at the start of the production run, but subsequent protonations to the pentyl carbenium ion are occasionally observed in the course of the production run. In the process, the acid proton may shift to a different framework oxygen around the Al defect. Proton jumps between neighboring oxygens of the zeolite framework have also been described in earlier theoretical studies [114–116]. Furthermore, frequent hydride shifts between the 2- and 3-pentyl carbenium ions take place, indicating that this isomerization is very low-activated at high temperature. In these simulations, the lifetime of the protonated state varies between 0.5 and 6 ps. These short lifetimes of the cationic state suggest that a linear carbenium ion may exist as metastable intermediate (rather than an activated transition state) at high temperature.

**Alkoxide simulations**

When starting from the 2-butoxide and 2-pentoxide at 323 K, both alkoxides remain stable during the entire simulation. At higher temperatures though, the covalent bond with the framework introduces an entropic penalty which can be expected to become increasingly important, resulting ultimately in cleavage of the C—O bond.

At 573 K, the covalent bond still remains in place throughout the entire simulation for 2-butoxide. 2-pentoxide on the other hand remains stable for 15.5 ps before transforming into a 2-pentyl carbenium ion, as shown in Fig. 4. As discussed before, the carbenium ion subsequently undergoes deprotonation after 2.1 ps forming a physisorbed 2-pentene.

As expected, at 773 K, rapid desorption of the 2-butoxide and 2-pentoxide from the acid site takes place at the start of the simulation, within the equilibration time (see Fig. 5). Upon desorption a carbenium ion is formed, which also rapidly transforms to the physisorbed π-complex. The enthalpic stabilization of the covalent C—O bond appears to be entirely compensated by the entropy loss. Therefore, no linear alkoxides are expected at high temperature. These findings provide interesting insights for other processes such as alkane hydrocracking. Thybaut et al. simulated octane hydrocracking via a single-event microkinetic model and found that carbocations are favored as reactive intermediates [117]. Bučko et al. studied propane dehydrogenation with transition path sampling and also arrived at the conclusion that carbenium ion formation is entropically favored over alkoxide formation [118].

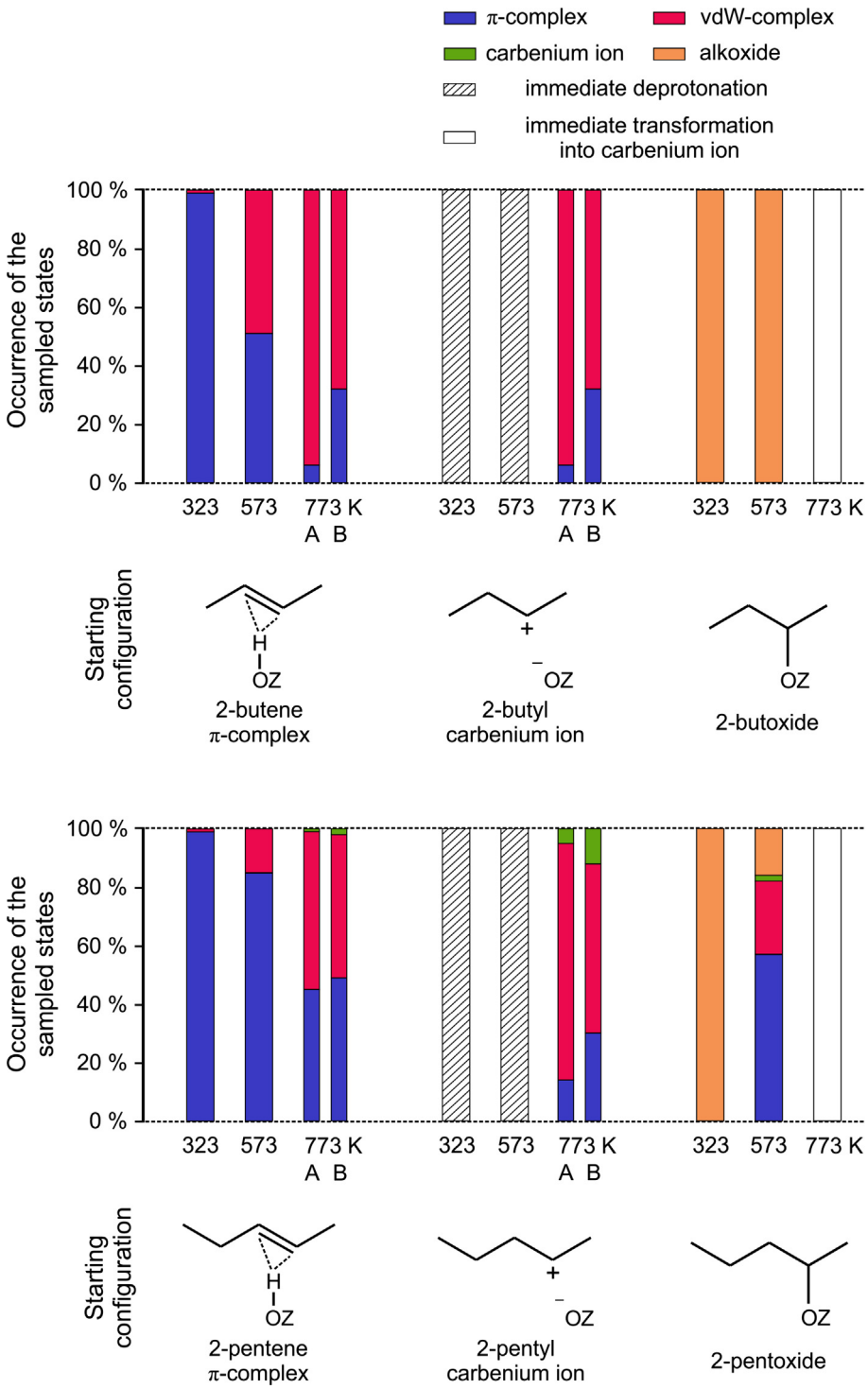


**Fig. 5.** Fractions of the occurring sampled intermediates during the 100 ps MD simulations on the linear $C_4$ and $C_5$ species at 323 K, 573 K and 773 K. Different simulations starting from the same configuration are indicated with A/B. When immediate transformations occurred, only the equilibration time was simulated.

*3.2.2. Branched C4 and C5 species*

**π-complex and carbenium ion simulations**

In sharp contrast to the linear alkenes, protonation into carbenium ions occurs in all branched $C_4$ and $C_5$ π-complex simulations (see Fig. 6). Even at 323 K, the free energy barrier between the π-complex and the carbenium ion is easily overcome and both states are sampled throughout the simulation. Simulations starting from a *tert*-butyl cation also confirmed the stable nature of tertiary carbenium ions. Again, regular transitions between the neutral and the protonated state take place.

The total sampling time of the carbenium ions encountered during the simulations, is also displayed in Fig. 6. At 773 K, during 90% of the total simulation time the system resides in a *tert*-butyl carbenium ion state with lifetimes fluctuating between 20 ps and 25 ps. During the remaining 10% of the simulation, deprotonations to isobutene occur, although not necessarily forming a π-complex. The freely adsorbed van der Waals complex is the most sampled state of deprotonated isobutene. At 573 K, the *tert*-butyl carbenium ion is sampled for more than 90 ps, regardless whether the simulation is started from a π-

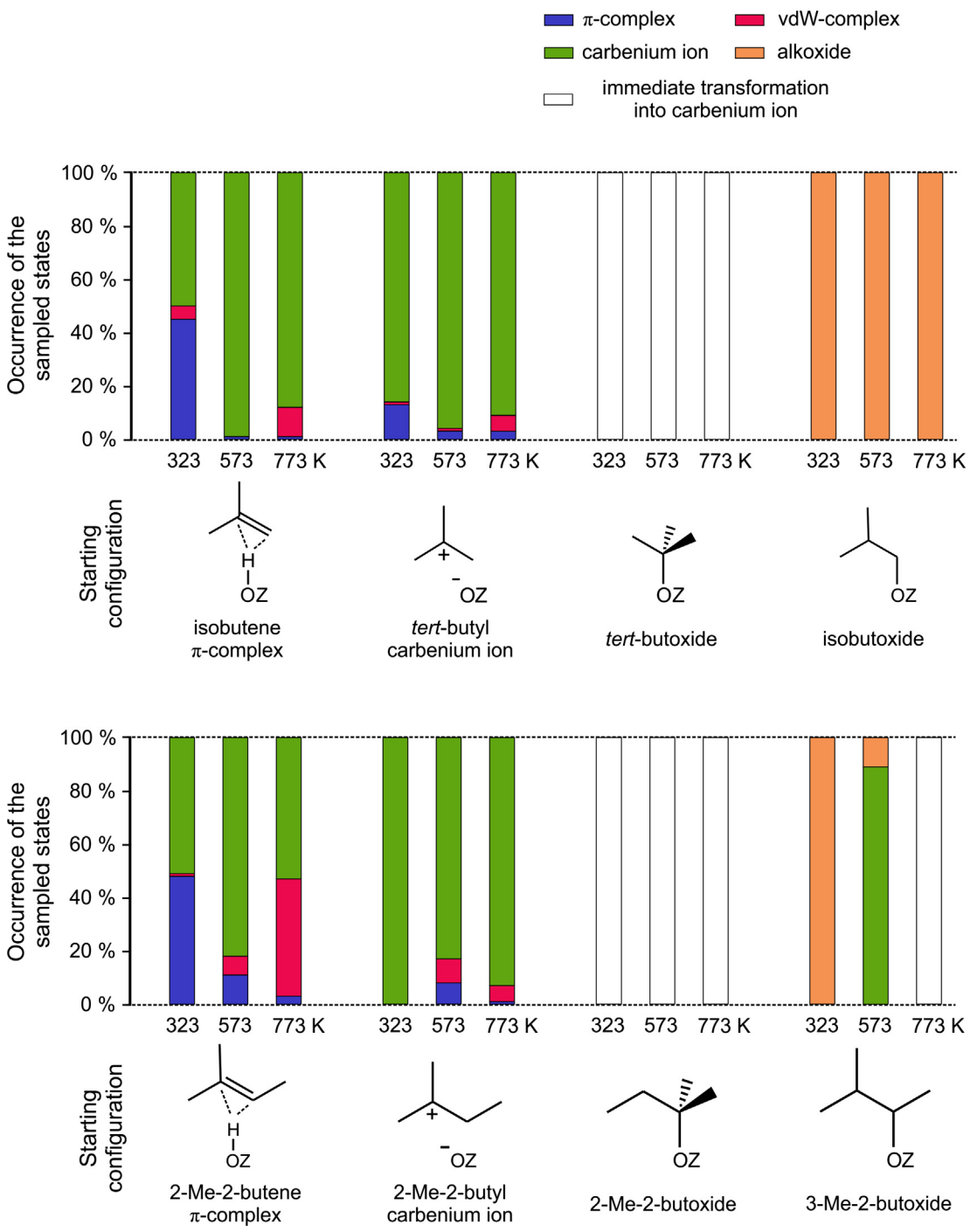


**Fig. 6.** Fractions of the occurring sampled intermediates during the 100 ps MD simulations on the branched $C_4$ and $C_5$ species at 323 K, 573 K and 773 K. When immediate transformations occurred, only the equilibration time was simulated.

complex or carbenium ion, while at 323 K, isobutene is visited to a larger extent, mostly as a π-complex.

The relative stability of protonated and neutral species clearly differs between the linear and the branched alkenes. The linear 2-pentyl carbenium ion was only rarely visited and the 2-butyl carbenium ion was not at all observed in any of the simulations. Instead, the *tert*-butyl carbenium ion is clearly more stable than the physisorbed isobutene, which has a shorter lifetime than the tertiary cation. This trend is not in agreement with our static calculations, in which the isobutene π-complex was systematically predicted to be lower in free energy than the *tert*-butyl carbenium ion. This discrepancy further emphasizes the limitations of a static approach relying on 0 K geometries and applying thermal corrections in the HO approximation. In reality, the carbenium ions will be much more mobile and larger portions of the free energy surface are accessible. Especially at the high temperatures encountered during cracking, one should be careful in relying solely on geometry optimizations at 0 K to predict stabilities of the reactive intermediates. Recently, schemes have been developed to account for the anharmonicity of the potential energy surface [119] but this is beyond the scope of this study.

For the $C_5$ species, large similarities with the $C_4$ species are observed for the various adsorption states shown in Fig. 6. Analogous to isobutene, branched pentene species will exist preferably as free van der Waals complexes instead of π-complexes at elevated temperatures. Three different $C_5$ alkene isomers can exist: 2-Me-1-butene, 3-Me-1-butene and 2-Me-2-butene. The latter has the most substituted double bond and is therefore the most stable of the three isomers. At 773 K, it is sampled for almost 50 ps before protonation. On the other hand, in the simulation starting from 2-Me-1-butene, protonation into the 2-methyl-2-butyl carbenium ion occurs after a sampling time of only 3 ps. In accordance with the high stability of the *tert*-butyl carbenium ion, the tertiary 2-Me-2-butyl carbenium ion is equally stable at all temperatures. The long-living carbenium ions are sampled during the main part of the production run with scarce transitions to the deprotonated 2-methyl-1-butene or 2-methyl-2-butene states. The lifetime of the 2-methyl-2-butyl cation ranges from 23 ps to 100 ps while the secondary 3-methyl-2-butyl cation is not sampled during the entire simulations, reflecting the considerable stability difference between tertiary and secondary carbenium ions.

Summarizing, tertiary carbenium ions thus exist as very stable reactive intermediates, both at high and low temperature, and will likely play an important role in catalytic cracking. This result supports the recent experiment of Dai et al. [71] who undoubtedly confirmed the formation of the *tert*-butyl cation during isobutene conversion on H-ZSM-5 by NMR spectroscopy after capturing with ammonia.

**Alkoxide simulations**

Upon isobutene adsorption, either the tertiary *tert*-butoxide or primary isobutoxide can be formed. Since the secondary 2-butoxide species was unstable at high temperature (773 K), a similar but more pronounced behavior can be expected for the tertiary butoxide which exhibits even more steric hindrance with the zeolite wall due to the additional methyl branch. Indeed, the covalent C—O bond immediately breaks at the start of the equilibration run, forming a *tert*-butyl cation. The extremely short sampling time of the *tert*-butoxide before desorption confirms the lower stability of this species. Even at intermediate (573 K) or low temperature (323 K), the alkoxide immediately desorbs. The unstable *tert*-butoxide will thus probably also not be formed as intermediate in the zeolite pores. This observation is in agreement with the static calculations, in which a positive free energy of adsorption for the *tert*-butoxide was already found at 323 K.

The stability order of alkoxides follows an opposite trend compared to the carbenium ions. Due to less steric hindrance with framework, a primary alkoxide is expected to be more stable than a secondary or tertiary alkoxide [19]. The higher stability of primary alkoxides is indeed confirmed for isobutoxide in our MD simulations. Throughout the entire 100 ps, the covalent bond remains in place, even at high temperature.

For the branched $C_5$ species, both tertiary 2-Me-2-butoxide and secondary 3-Me-2-butoxide can be formed as intermediates. The 2-Me-2-butoxide resembles a *tert*-butoxide with an additional methyl group. Consequently, the tertiary $C_5$ alkoxide is again very short-lived at all temperatures, transforming instantaneously into the more favorable 2-Me-2-butyl cation. The secondary 3-Me-2-butoxide is long-living at low temperature and unstable at high temperature, thus showing a similar behavior as the linear 2-pentoxide. At the intermediate transition temperature of 573 K, the 3-Me-2-butoxide was observed for 6 ps.

### 3.3. Determining free energy profiles of alkene adsorption with MTD simulations

Even at elevated temperatures, some regions of the free energy surface are scarcely or even not at all visited during regular MD. Some activation barriers are too high to overcome which may hinder sampling of the less probable regions. Using metadynamics (MTD) simulations, we try to reconstruct the free energy profile and to deduce activation barriers at 773 K for the transition from physisorbed alkene to chemisorbed carbenium ion and alkoxide. Table 3 summarizes the resulting forward and backward activation barriers, which are obtained as outlined in Section 2.4. Alternatively, the free energy barrier could also be calculated following a procedure proposed in previous work [69]. A complete overview of the simulations, including a comparison between both methods, is given in Section S7 of the Supplementary Material.

Note that the free energy profiles constructed from these simulations may be prone to variations induced by the choice of collective variable, size and positioning of the hills and additional phase space constraints. Given these possible uncertainties, the results should be regarded as indicative rather than accurate quantitative predictions. In an effort to eliminate these effects, each simulation was repeated 3–6 times and the average and spread of the resulting barriers are reported below. In the future, other advanced sampling techniques such as umbrella sampling [120–122] might be interesting to obtain more reliable barriers; however, this is beyond the scope of the current paper.

The MTD simulations corroborate the qualitative findings from the regular MD simulations. The alkene state in the MTD simulations is a combination of the physisorbed π-complex and physisorbed van der Waals complex. In Section 3.2.1, we discussed the frequent transitions and small barriers between these two states at high temperature, which justifies treating the physisorbed alkene states together as a single state. As expected, the linear alkene state is around 25 kJ/mol more stable than the cationic intermediate. A moderate activation barrier of ca. 23 kJ/mol separates the carbenium ion from the physisorbed alkene. This barrier can still be overcome in regular MD since the portion of the thermal energy corresponding to the reaction coordinate is sufficiently high. The transition from the 2-butyl or 2-pentyl carbenium into

**Table 3**
Free energy activation barriers and reaction free energy for the protonation of the different linear and branched alkenes into the corresponding carbenium ions at 773 K. Per reaction 5 or 6 MTD simulations have been performed unless explicitly specified.

| | $\Delta G^{\ddagger}_{fwd}$ (kJ/mol) | $\Delta G^{\ddagger}_{bwd}$ (kJ/mol) | $\Delta G_r$ (kJ/mol) |
|---|---|---|---|
| 2-butene → 2-butyl carbenium ion | 52 ± 4 | 23 ± 2 | 26 ± 5 |
| isobutene → *tert*-butyl carbenium ion | 25 ± 4 | 42 ± 6 | −17 ± 6 |
| 1-pentene → 2-pentyl carbenium ion | 37 ± 3 | 23 ± 4 | 14 ± 4 |
| 2-pentene → 2-pentyl carbenium ion | 49 ± 4 | 26 ± 2 | 23 ± 4 |
| 2-pentene → 3-pentyl carbenium ion | 49 ± 4 | 22 ± 6 | 27 ± 5 |
| 2-Me-2-butene → 2-Me-2-butyl carbenium ion[a] | 39 ± 11 | 50 ± 14 | −11 ± 10 |

[a] Only 3 simulations were performed.

**Table 4**
Free energy activation barriers and reaction free energy for the formation of the alkoxide from the corresponding carbenium ions at 773 K. Per reaction 5 or 6 MTD simulations have been performed unless explicitly specified.

| | $\Delta G^{\ddagger}_{fwd}$ (kJ/mol) | $\Delta G^{\ddagger}_{bwd}$ (kJ/mol) | $\Delta G_r$ (kJ/mol) |
|---|---|---|---|
| 2-pentyl carbenium ion → 2-pentoxide | 37 ± 7 | 16 ± 3 | 21 ± 4 |
| 3-pentyl carbenium ion → 3-pentoxide | 37 ± 4 | 13 ± 3 | 24 ± 5 |
| *tert*-butyl carbenium ion → *tert*-butoxide[a] | 91 | 3 | 88 |

[a] Only a single simulation was performed.

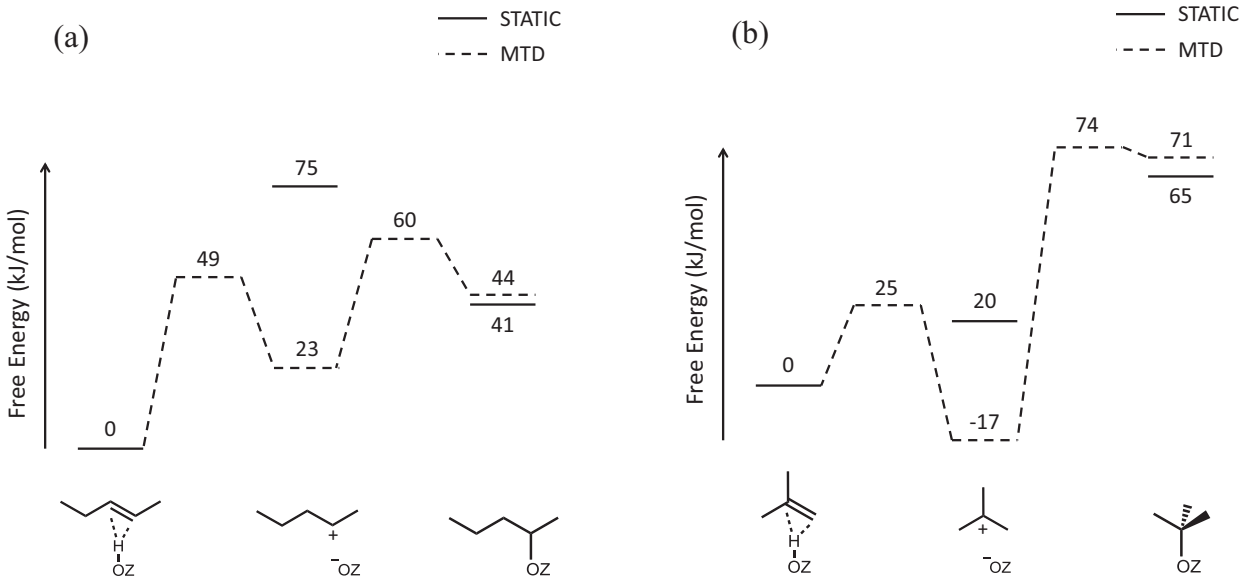


**Fig. 7.** Free energy profiles (kJ mol$^{-1}$) at 773 K for (a) the formation of 2-pentoxide from 2-pentene and for (b) the formation of tert-butoxide from isobutene (right) from 1D MTD simulations with indication of the static free energy estimates for the intermediates.

the deprotonated alkene is therefore likely to occur as already evidenced (*vide supra*).

The free energy barrier for protonation is somewhat higher than the barrier for deprotonation, explaining the long sampling times of the stable alkene state in MD with only rare transitions to the linear carbenium ion intermediates. Finally, the MTD simulations also indicate that physisorbed 1-pentene is less stable than physisorbed 2-pentene. The forward protonation barrier is clearly smaller for 1-pentene, while the deprotonation barriers transforming the 2-pentyl cation into 1-pentene or 2-pentene are almost equal.

In Section 3.2.1, we also found that linear alkoxides are unstable at typical cracking temperatures. Although alkoxides were not observed in regular MD, with metadynamics simulations the alkoxide state can be sampled, i.e., by forcing the carbenium ion to bind to the framework. To determine quantitatively the (in)stability of secondary alkoxides, MTD simulations were carried out on the formation of 2-pentoxide and 3-pentoxide. The results are reported in Table 4. Moderate activation barriers of 37 kJ/mol were found for the formation of these species. However, it should be stressed that alkoxide formation consists of two activated steps: first alkene protonation and secondly formation of a covalent bond between the resulting carbenium ion and the framework.

Furthermore, linear pentyl carbenium ions are ca. 20 kJ/mol more stabilized than the corresponding alkoxides. Despite the relatively small energy differences for the alkoxide formation, this transition was not sampled in the course of the MD simulations. This may be attributed to steric constraints, preventing the formation of an entropically disfavored covalent bond with the framework. Since the 3-pentoxide is fixed at its central carbon atom, its translational and rotational freedom is largely reduced, rendering it slightly less stable than the 2-pentoxide. The free energy profiles for these reactions are shown in Figs. 7a and 8b.

Fig. 7a shows the combined free energy profile at 773 K for the transition from 2-pentene over 2-pentyl carbenium ion into 2-pentoxide with indication of the static free energy levels for these intermediate states (cf. Section 3.1). The reaction free energies for 2-pentoxide and 3-pentoxide formation, derived from MTD are rather small (21 and 24 kJ/mol respectively) compared to the static calculations (−34 and −26 kJ/mol respectively). In particular, the carbenium ions were estimated much higher in free energy statically. These observations are in line with the regular MD findings. In reality, the carbenium ion intermediate can access a larger portion of the free energy surface at 773 K and is much more mobile than predicted from the 0 K geometry optimizations which only account for one state. Applying the HO approximation may underestimate the mobility and hence the entropy of the more loosely adsorbed intermediates such as the carbenium ion. For this reason, it can also be understood that the static estimate of the tightly bound alkoxide lies closer to the MTD value. To partially account for this effect, the Mobile Block Hessian (MBH) approach has been applied by De Moor et al. [123–125].

Regarding the branched species, we established in Section 3.2.2 that the stability order between the physisorbed alkene and carbenium ion is reversed. This observation is confirmed by the negative reaction free energies for the isobutene and 2-Me-2-butene protonation reactions. The tertiary carbenium ion is indeed quite stable and the deprotonation barriers amount to 42–50 kJ/mol, in agreement with the rare observations of these transitions in regular MD. The barrier for isobutene protonation is much lower than for 2-Me-2-butene protonation, showing again the stability difference between alkenes with a terminal double bond and a highly substituted double bond.

Tertiary alkoxides were shown to be extremely unstable at all temperatures due to steric constraints. To quantify this relative stability difference, we simulated the transition between the *tert*-butyl carbenium ion and the *tert*-butoxide (see Table 4). The latter appears to be almost 90 kJ/mol less stable than the *tert*-butyl cation. A very small barrier of 3 kJ/mol is required to break the covalent bond and restore the tertiary carbenium ion, thus explaining the rapid transitions in the MD simulations. In Figs. 7b and 8d, the free energy diagrams for this transition are plotted. In contrast to the alkoxides, once more the carbenium ion is better stabilized in the MTD simulations than predicted by our static calculations.

## 4. Conclusions

We have studied the nature of adsorbed $C_4$ and $C_5$ alkene intermediates in H-ZSM-5 at typical olefin cracking temperatures using a combination of static DFT calculations, molecular dynamics and metadynamics simulations. The relative stability of the different intermediates in an olefin cracking process – a physisorbed van der Waals complex, a physisorbed π-complex, a chemisorbed car-

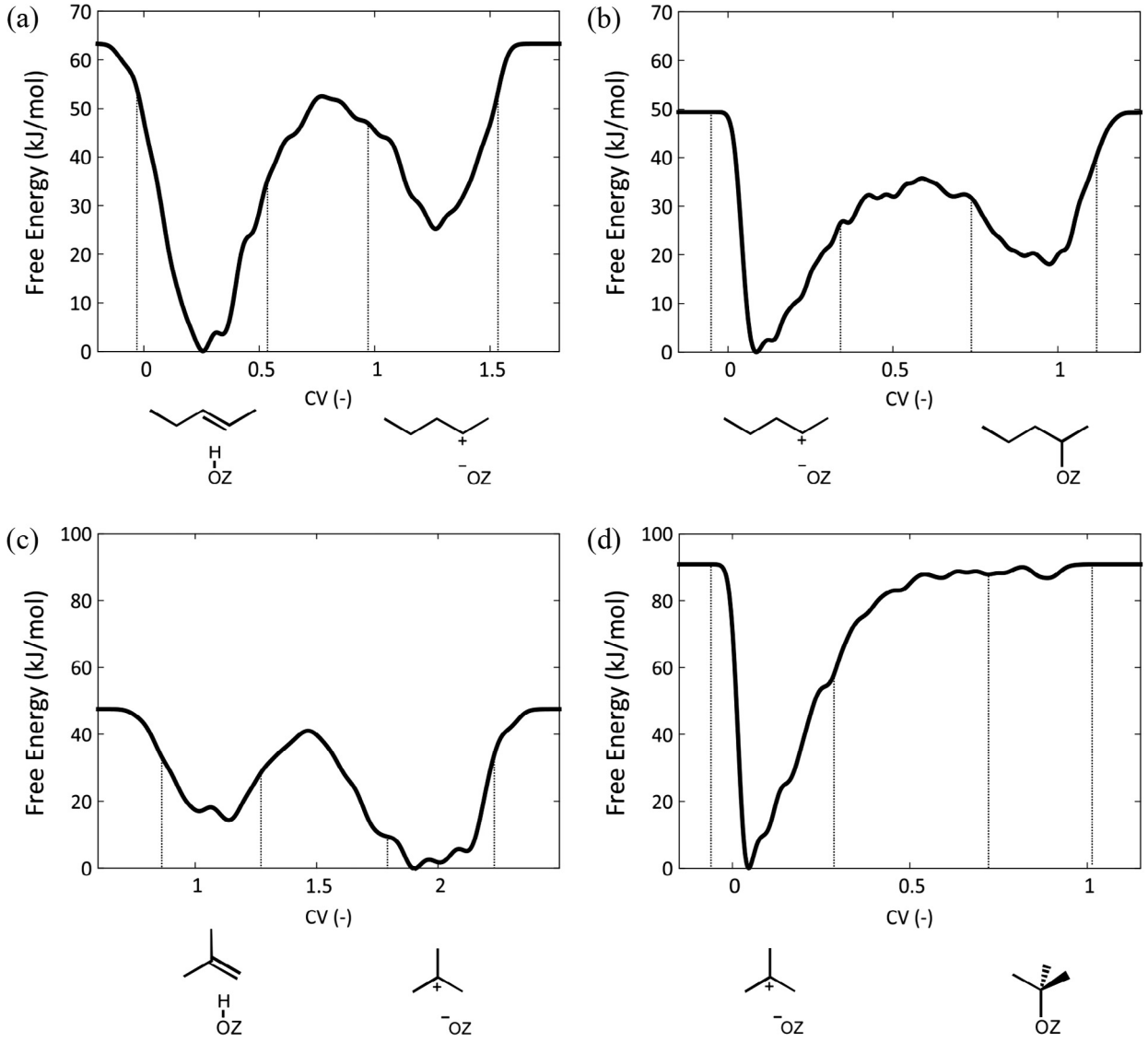


**Fig. 8.** 1D Free energy profiles at 773 K along the respective collective variable for (a) the transition from 2-pentene to 2-pentyl carbenium ion, (b) the transition from 2-pentyl carbenium ion to 2-pentoxide, (c) the transition from isobutene to *tert*-butyl carbenium ion and (d) the transition from *tert*-butyl carbenium ion to tert-butoxide.

benium ion or a chemisorbed alkoxide – was assessed. First, local minima on the potential energy surface were identified with static calculations. For linear alkenes at 773 K, π-complexes were found to be slightly more stable than alkoxides and far more stable than carbenium ions. For branched alkenes on the other hand, tertiary carbenium ions were predicted more stable than tertiary alkoxides, though still higher in energy than π-complexes.

To fully account for the mobility of the adsorbate and finite temperature effects, MD and MTD simulations have been applied. These simulations showed that the shape of the free energy surface is highly temperature dependent. For linear species at 323 K, both the alkene π-complex and alkoxide are very stable intermediates, while the carbenium ion seems extremely short-lived. At 773 K, however, the existence of alkoxides was found to be highly improbable. A more freely adsorbed state is favored, such as the metastable carbenium ion for the $C_5$ species. Furthermore, the π-complex is also less stable at high temperature and becomes competitive with the loosely bound van der Waals complex. Regular transitions between both physisorbed states were observed. The intermediate temperature of 573 K lies in the transition range between a stable and an unstable alkoxide regime. For branched alkenes on the other hand, different trends were identified. Tertiary carbenium ions are more favorable in free energy compared to the corresponding physisorbed alkene states at all temperatures. The sampling time of the *tert*-butyl carbenium ion increases with temperature. Interestingly, no tertiary alkoxides were observed, not even at low temperature. Primary alkoxides however may exist both at low and high temperatures.

We demonstrated that static calculations are not appropriate to estimate the nature and stability of the adsorbed species correctly at olefin cracking temperatures. Our MD results indicated that the stability of the alkoxide and π-complex structures may be overestimated in the static approach, while the carbenium ion stability may be underestimated. At high temperature, increased conformational freedom of the adsorbate and anharmonicity effects are expected to have an important effect.

In contrast to earlier predictions based on static calculations, we established that alkoxides are not the most stable or prevalent state in the zeolite channels at cracking conditions. Carbenium ions are much more stable than originally assumed and will probably play a crucial role as (meta)stable intermediates in the cracking process.

## Acknowledgments

PC, KDW, JVdM, MW and VVS acknowledge the Fund for Scientific Research – Flanders (FWO), the Research Board of Ghent University (BOF) and BELSPO in the frame of IAP/7/05 for financial support. VVS and KDW acknowledge funding from the European Union's Horizon 2020 research and innovation programme (consolidator ERC Grant Agreement No 647755 – DYNPOR (2015-2020)). The computational resources and services used in this work were provided by VSC (Flemish Supercomputer Center), funded by the Hercules foundation and the Flemish Government – department EWI.

## Appendix A. Supplementary material

Supplementary data associated with this article can be found, in the online version, at http://dx.doi.org/10.1016/j.jcat.2016.11.010.

## References

[1] M. Guisnet, J.-P. Gilson, Zeolites for Cleaner Technologies, Imperial College Press, London, 2002.
[2] W. Vermeiren, J.-P. Gilson, Impact of zeolites on the petroleum and petrochemical industry, Top. Catal. 52 (2009) 1131–1161.
[3] S. Ilias, A. Bhan, Mechanism of the catalytic conversion of methanol to hydrocarbons, ACS Catal. 3 (2013) 18–31.
[4] K. Hemelsoet, J. Van der Mynsbrugge, K. De Wispelaere, M. Waroquier, V. Van Speybroeck, Unraveling the reaction mechanisms governing methanol-to-olefins catalysis by theory and experiment, ChemPhysChem 14 (2013) 1526–1545.
[5] N. Rahimi, R. Karimzadeh, Catalytic cracking of hydrocarbons over modified ZSM-5 zeolites to produce light olefins: a review, Appl. Catal. Gen. 398 (2011) 1–17.
[6] H. Koempel, W. Liebner, Lurgi's methanol to propylene (MTP (R)) report on a successful commercialisation, Stud. Surf. Sci. Catal. 167 (2007) 261–267.
[7] O. Bortnovsky, P. Sazama, B. Wichterlova, Cracking of pentenes to C2–C4 light olefins over zeolites and zeotypes: role of topology and acid site strength and concentration, Appl. Catal. Gen. 287 (2005) 203–213.
[8] M.J. Tallman, C. Eng, Consider new catalytic routes for olefins production – innovative catalyst systems enable higher propylene make from liquid feedstocks, Hydrocarb. Process. 87 (2008) 95–101.
[9] J.Q. Chen, A. Bozzano, B. Glover, T. Fuglerud, S. Kvisle, Recent advancements in ethylene and propylene production using the UOP/hydro MTO process, Catal. Today 106 (2005) 103–107.
[10] J.S. Plotkin, The changing dynamics of olefin supply/demand, Catal. Today 106 (2005) 10–14.
[11] J. Abbot, B. Wojciechowski, The mechanism of catalytic cracking of normal-alkenes on Zsm-5 zeolite, Can. J. Chem. Eng. 63 (1985) 462–469.
[12] J.S. Buchanan, J.G. Santiesteban, W.O. Haag, Mechanistic considerations in acid-catalyzed cracking of olefins, J. Catal. 158 (1996) 279–287.
[13] J. Buchanan, The chemistry of olefins production by ZSM-5 addition to catalytic cracking units, Catal. Today 55 (2000) 207–212.
[14] A. Corma, A.V. Orchillés, Current views on the mechanism of catalytic cracking, Microporous Mesoporous Mater. 35–36 (2000) 21–30.
[15] Y.V. Kissin, Chemical mechanisms of catalytic cracking over solid acidic catalysts: alkanes and alkenes, Catal. Rev. 43 (2001) 85–146.
[16] C.M. Nguyen, B.A. De Moor, M.-F. Reyniers, G.B. Marin, Physisorption and chemisorption of linear alkenes in zeolites: a combined QM-Pot(MP2//B3LYP: GULP)–statistical thermodynamics study, J. Phys. Chem. C 115 (2011) 23831–23847.
[17] R.J. Correa, C.J.A. Mota, Theoretical study of protonation of butene isomers on acidic zeolite: the relative stability among primary, secondary and tertiary alkoxy intermediates, Phys. Chem. Chem. Phys. 4 (2002) 375–380.
[18] B.A. De Moor, M.-F. Reyniers, M. Sierka, J. Sauer, G.B. Marin, Physisorption and chemisorption of hydrocarbons in H-FAU using QM-Pot(MP2//B3LYP) calculations, J. Phys. Chem. C 112 (2008) 11796–11812.
[19] V. Nieminen, M. Sierka, D.Y. Murzin, J. Sauer, Stabilities of C3–C5 alkoxide species inside H-FER zeolite: a hybrid QM/MM study, J. Catal. 231 (2005) 393–404.
[20] A. Bhan, Y.V. Joshi, W.N. Delgass, K.T. Thomson, DFT investigation of alkoxide formation from olefins in H-ZSM-5, J. Phys. Chem. B 107 (2003) 10476–10487.
[21] A.M. Rigby, G.J. Kramer, R.A. van Santen, Mechanisms of hydrocarbon conversion in zeolites: a quantum mechanical study, J. Catal. 170 (1997) 1–10.
[22] M.N. Mazar, S. Al-Hashimi, M. Cococcioni, A. Bhan, β-Scission of olefins on acidic zeolites: a periodic PBE-D study in H-ZSM-5, J. Phys. Chem. C 117 (2013) 23609–23620.
[23] C.-J. Chen, S. Rangarajan, I.M. Hill, A. Bhan, Kinetics and thermochemistry of C4–C6 olefin cracking on H-ZSM-5, ACS Catal. 4 (2014) 2319–2327.
[24] Y.-X. Sun, J. Yang, L.-F. Zhao, J.-X. Dai, H. Sun, A two-layer ONIOM study on initial reactions of catalytic cracking of 1-butene to produce propene and ethene over HZSM-5 and HFAU zeolites, J. Phys. Chem. C 114 (2010) 5975–5984.
[25] C.-M. Wang, Y.-D. Wang, Z.-K. Xie, Insights into the reaction mechanism of methanol-to-olefins conversion in HSAPO-34 from first principles: Are olefins themselves the dominating hydrocarbon pool species?, J Catal. 301 (2013) 8–19.
[26] V. Van Speybroeck, K. Hemelsoet, L. Joos, M. Waroquier, R.G. Bell, C.R.A. Catlow, Advances in theory and their application within the field of zeolite chemistry, Chem. Soc. Rev. (2015) 7044–7111.
[27] K. De Wispelaere, S. Bailleul, V. Van Speybroeck, Towards molecular control of elementary reactions in zeolite catalysis by advanced molecular simulations mimicking operating conditions, Catal. Sci. Technol. 6 (2016) 2686–2705.
[28] J.F. Haw, B.R. Richardson, I.S. Oshiro, N.D. Lazo, J.A. Speed, Reactions of propene on zeolite HY catalyst studied by in situ variable temperature solid-state nuclear magnetic resonance spectroscopy, J. Am. Chem. Soc. 111 (1989) 2052–2058.
[29] N.D. Lazo, B.R. Richardson, P.D. Schettler, J.L. White, E.J. Munson, J.F. Haw, In situ variable-temperature MAS carbon-13 NMR study of the reactions of isobutylene in zeolites HY and HZSM-5, J. Phys. Chem. 95 (1991) 9420–9425.
[30] V.G. Mal'kin, V.V. Chesnokov, E. Paukstis, G.M. Zhidomirov, Quantum-chemical calculations of carbon-13 chemical shifts of the alkoxide form in zeolites, J. Am. Chem. Soc. 112 (1990) 666–669.
[31] J.F. Haw, J.B. Nicholas, T. Xu, L.W. Beck, D.B. Ferguson, Physical organic chemistry of solid acids: lessons from in situ NMR and theoretical chemistry, Acc. Chem. Res. 29 (1996) 259–267.
[32] A.G. Stepanov, K.I. Zamaraev, $^{13}$C solid state NMR evidence for the existence of isobutyl carbenium ion in the reaction of isobutyl alcohol dehydration in H-ZSM-5 zeolite, Catal. Lett. 19 (1993) 153–158.
[33] A.G. Stepanov, M.V. Luzgin, S.S. Arzumanov, H. Ernst, D. Freude, n-Butene conversion on H-Ferrierite studied by $^{13}$C MAS NMR, J. Catal. 211 (2002) 165–172.
[34] A.G. Stepanov, S.S. Arzumanov, M.V. Luzgin, H. Ernst, D. Freude, In situ monitoring of n-butene conversion on H-ferrierite by $^{1}$H, $^{2}$H, and $^{13}$C MAS NMR: kinetics of a double-bond-shift reaction, hydrogen exchange, and the $^{13}$C-label scrambling, J. Catal. 229 (2005) 243–251.
[35] F. Geobaldo, G. Spoto, S. Bordiga, C. Lamberti, A. Zecchina, Propene oligomerization on H-mordenite: hydrogen-bonding interaction, chain initiation, propagation and hydrogen transfer studied by temperature-programmed FTIR and UV–VIS spectroscopies, J. Chem. Soc. Faraday Trans. 93 (1997) 1243–1249.
[36] J.N. Kondo, S. Liqun, F. Wakabayashi, K. Domen, IR study of adsorption and reaction of 1-butene on H-ZSM-5, Catal. Lett. 47 (1997) 129–133.
[37] J.N. Kondo, K. Domen, F. Wakabayashi, Double bond migration of 1-butene without protonated intermediate on D-ZSM-5, Microporous Mesoporous Mater. 21 (1998) 429–437.
[38] J.N. Kondo, F. Wakabayashi, K. Domen, IR study of reaction of 2-butene adsorbed on deuterated ZSM-5 and mordenite, Catal. Lett. 53 (1998) 215–220.
[39] J.N. Kondo, F. Wakabayashi, K. Domen, IR study of adsorption of olefins on deuterated ZSM-5, J. Phys. Chem. B 102 (1998) 2259–2262.
[40] J.N. Kondo, H. Ishikawa, E. Yoda, F. Wakabayashi, K. Domen, Structure of dimerized alkoxy species of 2-methylpropene on zeolites and silica–alumina studied by FT-IR, J. Phys. Chem. B 103 (1999) 8538–8543.
[41] H. Ishikawa, E. Yoda, J.N. Kondo, F. Wakabayashi, K. Domen, Stable dimerized alkoxy species of 2-methylpropene on mordenite zeolite studied by FT-IR, J. Phys. Chem. B 103 (1999) 5681–5686.
[42] M. Boronat, P. Viruela, A. Corma, Theoretical study of the mechanism of zeolite-catalyzed isomerization reactions of linear butenes, J. Phys. Chem. A 102 (1998) 982–989.
[43] V.B. Kazansky, The nature of adsorbed carbenium ions as active intermediates in catalysis by solid acids, Acc. Chem. Res. 24 (1991) 379–383.
[44] P. Jeffrey Hay, A. Redondo, Y. Guo, Theoretical studies of pentene cracking on zeolites: C—C β-scission processes, Catal. Today 50 (1999) 517–523.
[45] A.M. Rigby, M.V. Frash, Ab initio calculations on the mechanisms of hydrocarbon conversion in zeolites: skeletal isomerisation and olefin chemisorption, J. Mol. Catal. Chem. 126 (1997) 61–72.
[46] M.V. Frash, R.A. van Santen, Quantum-chemical modeling of the hydrocarbon transformations in acid zeolite catalysts, Top. Catal. 9 (1999) 191–205.
[47] M.V. Frash, V.B. Kazansky, A.M. Rigby, R.A. van Santen, Cracking of hydrocarbons on zeolite catalysts: density functional and Hartree–Fock calculations on the mechanism of the β-scission reaction, J. Phys. Chem. B 102 (1998) 2232–2238.
[48] S.R. Blaszkowski, M.A.C. Nascimento, R.A. van Santen, Activation of C—H and C—C bonds by an acidic zeolite: a density functional study, J. Phys. Chem. 100 (1996) 3463–3472.
[49] W. Wang, M. Hunger, Reactivity of surface alkoxy species on acidic zeolite catalysts, Acc. Chem. Res. 41 (2008) 895–904.
[50] V.B. Kazansky, Adsorbed carbocations as transition states in heterogeneous acid catalyzed transformations of hydrocarbons, Catal. Today 51 (1999) 419–434.
[51] M. Boronat, C.M. Zicovich-Wilson, P. Viruela, A. Corma, Influence of the local geometry of zeolite active sites and olefin size on the stability of alkoxide intermediates, J. Phys. Chem. B 105 (2001) 11169–11177.

[52] Y. Chu, B. Han, A. Zheng, X. Yi, F. Deng, Pore selectivity for olefin protonation reactions confined inside mordenite zeolite: a theoretical calculation study, J. Phys. Chem. C 117 (2013) 2194–2202.
[53] S. Svelle, S. Kolboe, O. Swang, Theoretical investigation of the dimerization of linear alkenes catalyzed by acidic zeolites, J. Phys. Chem. B 108 (2004) 2953–2962.
[54] M. Boronat, P.M. Viruela, A. Corma, Reaction intermediates in acid catalysis by zeolites: prediction of the relative tendency to form alkoxides or carbocations as a function of hydrocarbon nature and active site structure, J. Am. Chem. Soc. 126 (2004) 3300–3309.
[55] M. Boronat, A. Corma, Are carbenium and carbonium ions reaction intermediates in zeolite-catalyzed reactions?, Appl Catal. Gen. 336 (2008) 2–10.
[56] H. Fang, A. Zheng, S. Li, J. Xu, L. Chen, F. Deng, New Insights into the effects of acid strength on the solid acid-catalyzed reaction: theoretical calculation study of olefinic hydrocarbon protonation reaction, J. Phys. Chem. C 114 (2010) 10254–10264.
[57] H. Fang, A. Zheng, J. Xu, S. Li, Y. Chu, L. Chen, F. Deng, Theoretical investigation of the effects of the zeolite framework on the stability of carbenium ions, J. Phys. Chem. C 115 (2011) 7429–7439.
[58] C.M. Nguyen, B.A. De Moor, M.-F. Reyniers, G.B. Marin, Isobutene protonation in H-FAU, H-MOR, H-ZSM-5, and H-ZSM-22, J. Phys. Chem. C 116 (2012) 18236–18249.
[59] Y.-H. Guo, M. Pu, B.-H. Chen, F. Cao, Theoretical study on the cracking reaction catalyzed by a solid acid with zeolitic structure: the catalytic cracking of 1-hexene on the surface of H-ZSM-5, Appl. Catal. Gen. 455 (2013) 65–70.
[60] L. Benco, J. Hafner, F. Hutschka, H. Toulhoat, Physisorption and chemisorption of some n-hydrocarbons at the Brønsted acid site in zeolites 12-membered ring main channels: Ab initio study of the gmelinite structure, J. Phys. Chem. B 107 (2003) 9756–9762.
[61] C. Tuma, T. Kerber, J. Sauer, The *tert*-butyl cation in H-zeolites: deprotonation to isobutene and conversion into surface alkoxides, Angew. Chem. Int. Ed. 49 (2010) 4678–4680.
[62] G.A. Ferguson, L. Cheng, L. Bu, S. Kim, D.J. Robichaud, M.R. Nimlos, L.A. Curtiss, G.T. Beckham, Carbocation stability in H-ZSM5 at high temperature, J. Phys. Chem. A 119 (2015) 11397–11405.
[63] A.L.L. East, T. Bučko, J. Hafner, On the structure and dynamics of secondary n-alkyl cations, J. Chem. Phys. 131 (2009) 104314.
[64] J.B. Nicholas, J.F. Haw, The prediction of persistent carbenium ions in zeolites, J. Am. Chem. Soc. 120 (1998) 11804–11805.
[65] L.A. Clark, M. Sierka, J. Sauer, Stable mechanistically-relevant aromatic-based carbenium ions in zeolite catalysts, J. Am. Chem. Soc. 125 (2003) 2136–2141.
[66] S. Svelle, M. Bjørgen, Mechanistic proposal for the zeolite catalyzed methylation of aromatic compounds, J. Phys. Chem. A 114 (2010) 12548–12554.
[67] L. Benco, T. Demuth, J. Hafner, F. Hutschka, H. Toulhoat, Linear hydrocarbons adsorbed in the acid zeolite gmelinite at 700 K ab initio molecular dynamics simulation of hexane and hexene, J. Catal. 205 (2002) 147–156.
[68] F. Göltl, J. Hafner, Modelling the adsorption of short alkanes in protonated chabazite: the impact of dispersion forces and temperature, Microporous Mesoporous Mater. 166 (2013) 176–184.
[69] J. Hajek, J. Van der Mynsbrugge, K. De Wispelaere, P. Cnudde, L. Vanduyfhuys, M. Waroquier, V. Van Speybroeck, On the stability and nature of adsorbed pentene in Brønsted acid zeolite H-ZSM-5 at 323 K, J. Catal. 340 (2016) 227–235.
[70] C. Tuma, J. Sauer, Protonated isobutene in zeolites: tert-Butyl cation or alkoxide?, Angew Chem. 117 (2005) 4847–4849.
[71] W. Dai, C. Wang, X. Yi, A. Zheng, L. Li, G. Wu, N. Guan, Z. Xie, M. Dyballa, M. Hunger, Identification of *tert*-butyl cations in zeolite H-ZSM-5: evidence from NMR Spectroscopy and DFT calculations, Angew. Chem. Int. Ed. 54 (2015) 8783–8786.
[72] N. Rosenbach Jr., A.P.A. dos Santos, M. Franco, C.J.A. Mota, The *tert*-butyl cation on zeolite Y: a theoretical and experimental study, Chem. Phys. Lett. 485 (2010) 124–128.
[73] X. Rozanska, R.A. van Santen, T. Demuth, F. Hutschka, J. Hafner, A periodic DFT study of isobutene chemisorption in proton-exchanged zeolites: dependence of reactivity on the zeolite framework structure, J. Phys. Chem. B 107 (2003) 1309–1315.
[74] C. Tuma, J. Sauer, Treating dispersion effects in extended systems by hybrid MP2: DFT calculations—protonation of isobutene in zeolite ferrierite, Phys. Chem. Chem. Phys. 8 (2006) 3955–3965.
[75] M.A. den Hollander, M. Wissink, M. Makkee, J.A. Moulijn, Gasoline conversion: reactivity towards cracking with equilibrated FCC and ZSM-5 catalysts, Appl. Catal. Gen. 223 (2002) 85–102.
[76] X. Zhu, S. Liu, Y. Song, L. Xu, Catalytic cracking of C4 alkenes to propene and ethene: influences of zeolites pore structures and $Si/Al_2$ ratios, Appl. Catal. Gen. 288 (2005) 134–142.
[77] T. von Aretin, O. Hinrichsen, Single-event kinetic model for cracking and isomerization of 1-hexene on ZSM-5, Ind. Eng. Chem. Res. 53 (2014) 19460–19470.
[78] T. von Aretin, S. Schallmoser, S. Standl, M. Tonigold, J.A. Lercher, O. Hinrichsen, Single-event kinetic model for 1-pentene cracking on ZSM-5, Ind. Eng. Chem. Res. 54 (2015) 11792–11803.
[79] V. Van Speybroeck, K. De Wispelaere, J. Van der Mynsbrugge, M. Vandichel, K. Hemelsoet, M. Waroquier, First principle chemical kinetics in zeolites: the methanol-to-olefin process as a case study, Chem. Soc. Rev. 43 (2014) 7326–7357.
[80] S.L.C. Moors, K. De Wispelaere, J. Van der Mynsbrugge, M. Waroquier, V. Van Speybroeck, Molecular dynamics kinetic study on the zeolite-catalyzed benzene methylation in ZSM-5, ACS Catal. 3 (2013) 2556–2567.
[81] J. Van der Mynsbrugge, S.L.C. Moors, K. De Wispelaere, V. Van Speybroeck, Insight into the formation and reactivity of framework-bound methoxide species in H-ZSM-5 from static and dynamic molecular simulations, ChemCatChem 6 (2014) 1906–1918.
[82] P.M. Zimmerman, D.C. Tranca, J. Gomes, D.S. Lambrecht, M. Head-Gordon, A.T. Bell, Ab initio simulations reveal that reaction dynamics strongly affect product selectivity for the cracking of alkanes over H-MFI, J. Am. Chem. Soc. 134 (2012) 19468–19476.
[83] T. Jiang, F. Göltl, R.E. Bulo, P. Sautet, Effect of temperature on the adsorption of short alkanes in the zeolite SSZ-13—adapting adsorption isotherms to microporous materials, ACS Catal. 4 (2014) 2351–2358.
[84] T. Bučko, L. Benco, J. Hafner, J.G. Ángyán, Monomolecular cracking of propane over acidic chabazite: an ab initio molecular dynamics and transition path sampling study, J. Catal. 279 (2011) 220–228.
[85] E. Sandre, M.C. Payne, I. Stich, Determination of transition state structures using large scale Ab-initio techniques, in: K. Morokuma, D.G. Truhlar (Eds.), ACS Symp. Ser., Washington DC, 1999, pp. 358–367.
[86] J. Sauer, M. Sierka, F. Haase, Transitions state modeling for catalysis, in: K. Morokuma, D.G. Truhlar (Eds.), ACS Symp. Ser., Washington DC, 1999, pp. 358–367.
[87] G. Kresse, J. Hafner, Ab initio molecular dynamics for liquid metals, Phys. Rev. B 47 (1993) 558–561.
[88] G. Kresse, J. Hafner, Ab initio molecular-dynamics simulation of the liquid-metal amorphous-semiconductor transition in germanium, Phys. Rev. B 49 (1994) 14251–14269.
[89] G. Kresse, J. Furthmüller, Efficiency of ab-initio total energy calculations for metals and semiconductors using a plane-wave basis set, Comput. Mater. Sci. 6 (1996) 15–50.
[90] G. Kresse, J. Furthmüller, Efficient iterative schemes for ab initio total-energy calculations using a plane-wave basis set, Phys. Rev. B 54 (1996) 11169–11186.
[91] S. Grimme, J. Antony, S. Ehrlich, H. Krieg, A consistent and accurate ab initio parametrization of density functional dispersion correction (DFT-D) for the 94 elements H-Pu, J. Chem. Phys. 132 (2010) 154104.
[92] G. Kresse, D. Joubert, From ultrasoft pseudopotentials to the projector augmented-wave method, Phys. Rev. B 59 (1999) 1758–1775.
[93] P.E. Blöchl, Projector augmented-wave method, Phys. Rev. B 50 (1994) 17953–17979.
[94] A. Ambrosetti, A.M. Reilly, R.A. Jr. DiStasio, A. Tkatchenko, Long-range correlation energy calculated from coupled atomic response functions, J. Chem. Phys. 140 (2014) 18A508.
[95] T. Bučko, S. Lebègue, T. Gould, J.G. Ángyán, Many-body dispersion corrections for periodic systems: an efficient reciprocal space implementation, J. Phys. Condens. Matter. 28 (2016).
[96] A. Ghysels, D. Van Neck, M. Waroquier, Cartesian formulation of the mobile block Hessian approach to vibrational analysis in partially optimized systems, J. Chem. Phys. 127 (2007) 164108.
[97] M.T. Reetz, A. Meiswinkel, G. Mehler, K. Angermund, M. Graf, W. Thiel, R. Mynott, D.G. Blackmond, Why are BINOL-based monophosphites such efficient ligands in Rh-catalyzed asymmetric olefin hydrogenation?, J Am. Chem. Soc. 127 (2005) 10305–10313.
[98] P.J. Donoghue, P. Helquist, P.-O. Norrby, O. Wiest, Development of a Q2MM force field for the asymmetric rhodium catalyzed hydrogenation of enamides, J. Chem. Theory Comput. 4 (2008) 1313–1323.
[99] A. Ghysels, T. Verstraelen, K. Hemelsoet, M. Waroquier, V. Van Speybroeck, TAMkin: a versatile package for vibrational analysis and chemical kinetics, J. Chem. Inf. Model. 50 (2010) 1736–1750.
[100] J. VandeVondele, M. Krack, F. Mohamed, M. Parrinello, T. Chassaing, J. Hutter, QUICKSTEP: fast and accurate density functional calculations using a mixed Gaussian and plane waves approach, Comput. Phys. Commun. 167 (2005) 103–128.
[101] J. Hutter, M. Iannuzzi, F. Schiffmann, J. VandeVondele, Cp2k: atomistic simulations of condensed matter systems, Wiley Interdiscip. Rev. Comput. Mol. Sci. 4 (2014) 15–25.
[102] K. Yang, J. Zheng, Y. Zhao, D.G. Truhlar, Tests of the RPBE, revPBE, τ-HCTHhyb, ωB97X-D, and MOHLYP density functional approximations and 29 others against representative databases for diverse bond energies and barrier heights in catalysis, J. Chem. Phys. 132 (2010) 164117.
[103] S. Goedecker, M. Teter, J. Hutter, Separable dual-space Gaussian pseudopotentials, Phys. Rev. B 54 (1996) 1703–1710.
[104] G. Lippert, J. Hutter, M. Parrinello, The Gaussian and augmented-plane-wave density functional method for ab initio molecular dynamics simulations, Theor. Chem. Acc. 103 (1999) 124–140.
[105] G. Lippert, J. Hutter, M. Parrinello, A hybrid Gaussian and plane wave density functional scheme, Mol. Phys. 92 (1997) 477–488.
[106] S. Nosé, A molecular dynamics method for simulations in the canonical ensemble, Mol. Phys. 52 (1984) 255–268.
[107] G.J. Martyna, M.L. Klein, M. Tuckerman, Nosé–Hoover chains: the canonical ensemble via continuous dynamics, J. Chem. Phys. 97 (1992) 2635–2643.
[108] G.J. Martyna, D.J. Tobias, M.L. Klein, Constant pressure molecular dynamics algorithms, J. Chem. Phys. 101 (1994) 4177–4189.

[109] A. Laio, M. Parrinello, Escaping free-energy minima, Proc. Natl. Acad. Sci. 99 (2002) 12562–12566.
[110] A. Laio, F.L. Gervasio, Metadynamics: a method to simulate rare events and reconstruct the free energy in biophysics, chemistry and material science, Rep. Prog. Phys. 71 (2008) 126601.
[111] G. Bussi, A. Laio, M. Parrinello, Equilibrium free energies from nonequilibrium metadynamics, Phys. Rev. Lett. 96 (2006) 90601.
[112] T. Kerber, M. Sierka, J. Sauer, Application of semiempirical long-range dispersion corrections to periodic systems in density functional theory, J. Comput. Chem. 29 (2008) 2088–2097.
[113] S. Grimme, Semiempirical GGA-type density functional constructed with a long-range dispersion correction, J. Comput. Chem. 27 (2006) 1787–1799.
[114] Ľ. Benco, T. Demuth, J. Hafner, F. Hutschka, Spontaneous proton transfer between O-sites in zeolites, Chem. Phys. Lett. 324 (2000) 373–380.
[115] M. Sierka, J. Sauer, Proton mobility in Chabazite, Faujasite, and ZSM-5 zeolite catalysts. Comparison based on ab initio calculations, J. Phys. Chem. B 105 (2001) 1603–1613.
[116] C. Tuma, J. Sauer, A hybrid MP2/planewave-DFT scheme for large chemical systems: proton jumps in zeolites, Chem. Phys. Lett. 387 (2004) 388–394.
[117] J.W. Thybaut, C.S.L. Narasimhan, G.B. Marin, J.F.M. Denayer, G.V. Baron, P.A. Jacobs, J.A. Martens, Alkylcarbenium ion concentrations in zeolite pores during octane hydrocracking on Pt/H-USY zeolite, Catal. Lett. 94 (2004) 81–88.
[118] T. Bučko, L. Benco, O. Dubay, C. Dellago, J. Hafner, Mechanism of alkane dehydrogenation catalyzed by acidic zeolites: Ab initio transition path sampling, J. Chem. Phys. 131 (2009) 214508.
[119] G. Piccini, J. Sauer, Effect of anharmonicity on adsorption thermodynamics, J. Chem. Theory Comput. 10 (2014) 2479–2487.
[120] J. Kästner, Umbrella sampling, Wiley Interdiscip. Rev. Comput. Mol. Sci. 1 (2011) 932–942.
[121] C. Abrams, G. Bussi, Enhanced sampling in molecular dynamics using metadynamics, replica-exchange, and temperature-acceleration, Entropy 16 (2013) 163–199.
[122] G.M. Torrie, J.P. Valleau, Nonphysical sampling distributions in Monte Carlo free-energy estimation: umbrella sampling, J. Comput. Phys. 23 (1977) 187–199.
[123] A. Ghysels, D. Van Neck, V. Van Speybroeck, T. Verstraelen, M. Waroquier, Vibrational modes in partially optimized molecular systems, J. Chem. Phys. 126 (2007) 224102.
[124] B.A. De Moor, A. Ghysels, M.-F. Reyniers, V. Van Speybroeck, M. Waroquier, G. B. Marin, Normal mode analysis in zeolites: toward an efficient calculation of adsorption entropies, J. Chem. Theory Comput. 7 (2011) 1090–1101.
[125] B.A. De Moor, M.-F. Reyniers, G.B. Marin, Physisorption and chemisorption of alkanes and alkenes in H-FAU: a combined ab initio–statistical thermodynamics study, Phys. Chem. Chem. Phys. 11 (2009) 2939–2958.